NTNU

Norwegian University of
Science and Technology

Kinetic study of high temperature water gas shift reaction

Damien Vannier

Chemical Engineering
Submission date: June 2011
Supervisor: De Chen, IKP

Norwegian University of Science and Technology
Department of Chemical Engineering

Acknowledgement

I would like to thank my supervisor, Professor De Chen, for his support and his help during the progression of my project.

A special thank goes to Jun Zhu, Postdoctoral fellow, for his help with the set up and his suggestions.

I'm also thankful to Tayyaba Noor, Phd student, for sharing her results and her catalysts.

Finally I would like to thank all the NTNU workers without whom nothing would be possible.

Table of content

Summary

The water gas shift reaction has been run at high temperature in a packed bed reactor with a nickel catalyst. The outlet was analyzed by gas chromatography. Gas phase reaction and diffusion limitations appeared to be significant problems for a kinetic study. Rate expressions for different mechanisms have been given in order to find a coherent pathway for the water gas shift reaction over nickel. From the reaction orders of hydrogen and carbon monoxide it was concluded that the redox mechanism was valid at high temperature over nickel with the carbon dioxide formation as the rate determining step. Moreover effect of the diffusion was highlighted by the comparison of the apparent activation energy under chemical and diffusion control. The addition of cobalt in the catalyst showed a better selectivity for the water gas shift reaction.

Introduction

Hydrogen production is an important step in many industrial processes (ammonia production, methanol production, sulfur removal in oil refineries), and it is becoming more significant in an energy context because of the application of hydrogen as an energy carrier, for example in fuel cells.

Currently the most common way to produce hydrogen is the steam reforming of natural gas, but other ways are known and studied, such as electrolysis of water, biomass gasification or photocatalysis.

The steam reforming is currently the least expensive method and the most used.

$$CH_4 + H_2O \leftrightarrow CO + 3H_2$$

This reaction is endothermic (ΔH=206 kJ.mol^{-1}) and occurs at high temperature (600°C-1000°C) on a nickel-based catalyst. It is followed by the water gas shift reaction to convert the carbon monoxide produced into more hydrogen.

$$CO + H_2O \leftrightarrow CO_2 + H_2$$

This exothermic reaction (ΔH=-41 kJ.mol^{-1}) is used in two stages, first at high temperature (310°C-450°C) and then at lower temperature (210°C-250°C).

The object of this study is the high temperature shift on a nickel catalyst.

I.LITERATURE REVIEW

As the water gas shift reaction is important in the industry and is used for more than 50 years, it has been the subject of many articles and chapters in books from the beginning of its industrial use [1-7]. The recent concerns about clean energy and hydrogen production have led to a renewed interest in the water gas shift reaction over the past few years. The water gas shift reaction for fuel cells applications is now studied [8] in addition to the traditional use of this reaction (ammonia and methanol production).

The publications can be divided into two types of studies: those about composition and structure of the catalysts for water gas shift reaction, and those about the kinetics and mechanism of the water gas shift reaction. Both subjects have been studied a lot, so a wide range of data is available for different catalysts, and at different conditions. Despite the large number of studies concerning the mechanism of the water gas shift reaction, there is no consensus about it and the kinetics and the mechanisms are still discussed.

I.1.Thermodynamics

The water gas shift reaction is equilibrated. Its equilibrium constant can be expressed like this: $K = \frac{P_{H2}P_{CO2}}{P_{CO}P_{H2O}}$.

The effect of the temperature is given by: $K = exp\left(\frac{4577,8}{T} - 4,33\right)$ [Moe (1962)].

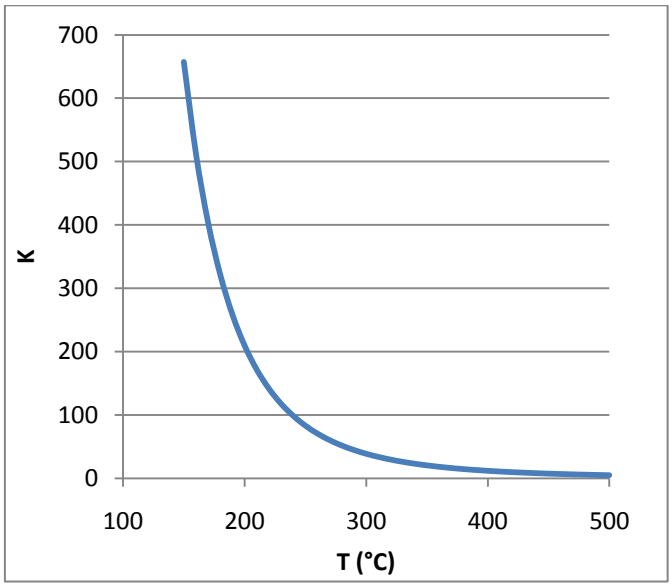

Figure 1: Effect of the temperature on the equilibrium constant of the WGSR

The equilibrium constant decreases as the temperature increases. So the reaction is thermodynamically favored at low temperatures and kinetically favored at high temperatures. The solution is to use a catalyst, which will allow working at lower temperature for the same conversion.

It is useful to note that the pressure doesn't influence the equilibrium since there is no variation in the gas number of mole during the reaction.

I.2.Industrial use

The water gas shift reaction is used extensively in the industry to produce hydrogen with high purity like in the ammonia synthesis process. It is also used to remove CO like in fuel cells.

I.2.1.Haber-Bosch process

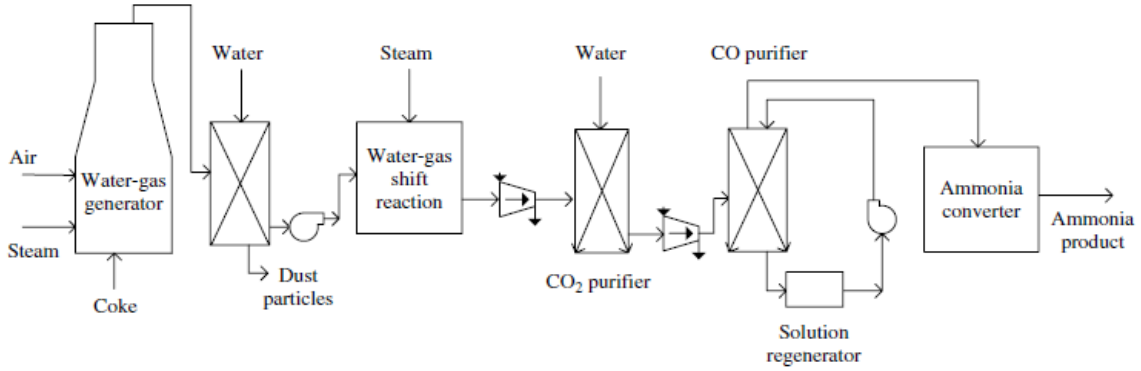

Figure 2: Haber-Bosch process for ammonia synthesis

Ammonia synthesis in the industry is performed by the Haber-Bosch process, named based on its inventors. The ammonia synthesis process consists in the reaction of nitrogen with hydrogen to form ammonia over an iron catalyst:

$$3H_2 + N_2 \rightarrow 2NH_3$$

The Haber-Bosch process needs large quantities of hydrogen that is provided by steam reforming.

I.2.2.Steam reforming

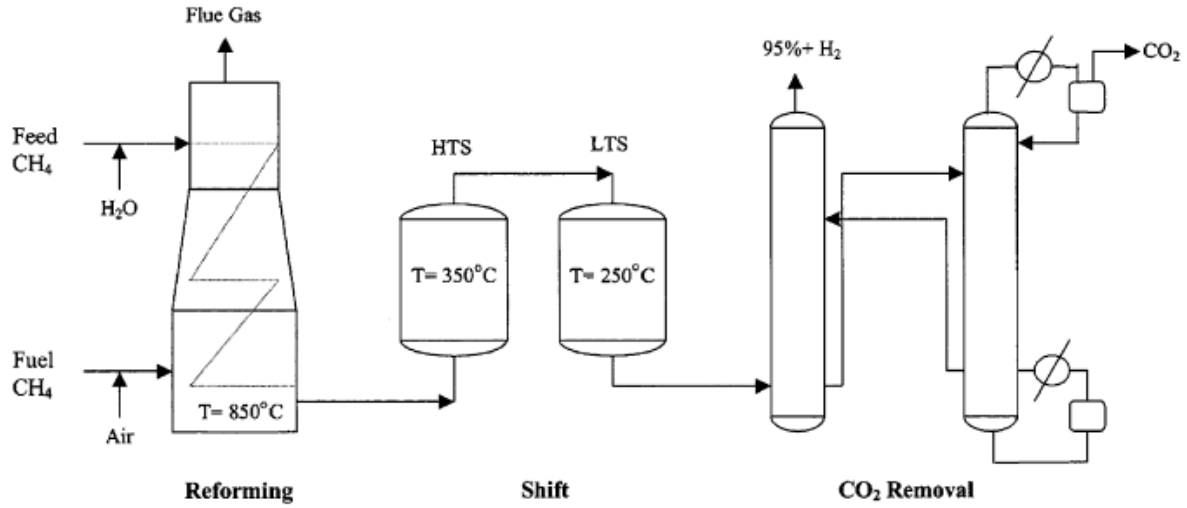

Figure 3: Steam methane reforming process

Hydrogen is mainly produced by steam reforming of natural gas, i.e. methane, hydrocarbons like propane or butane:

$$CH_4 + H_2O \rightarrow CO + 3H_2$$

$$CH_4 + 2H_2O \rightarrow CO_2 + 4H_2$$

The next step is the water gas shift reaction to convert the carbon monoxide into carbon dioxide and more hydrogen. It is performed in two consecutive reactors, the first at high temperature and the second at low temperature. Adiabatic fixed bed reactors are used in both steps. The first stage is called high temperature shift and is run over Fe_2O_3/Cr_2O_3 at temperatures between 310°C and 450°C. This allows a quick conversion but due to the thermodynamics the conversion reached is not high. The second stage, the low temperature shift, is at temperature around 200°C over CuO-ZnO/Al_2O_3 and it converts the remaining CO of the exit of the HTS since the equilibrium conversion is higher for low temperatures.

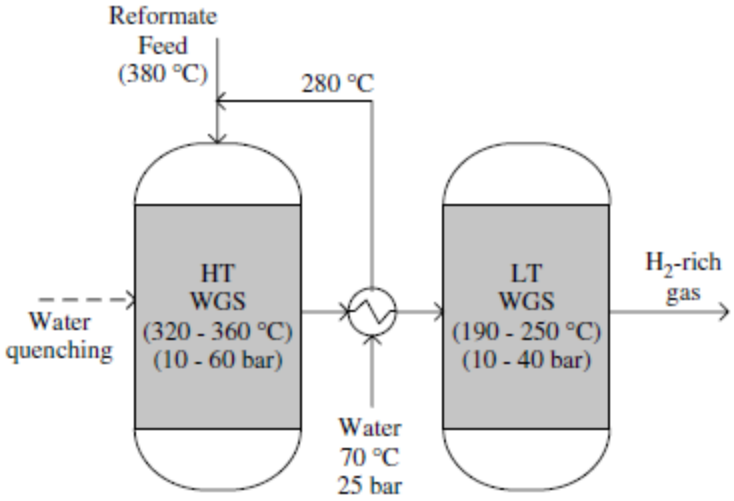

Figure 4: The two stages of the water gas shift reaction

A CO_2 and a CO removal unit are often placed after the WATER GAS SHIFT REACTION in order to purify the hydrogen before using it for synthesis. Carbon dioxide can be removed by absorption or adsorption and then catalytic methanation is used to remove the residual traces of CO and CO_2:

$$CO + 3H_2 \rightarrow CH_4 + H_2O$$

$$CO_2 + 4H_2 \rightarrow CH_4 + 2H_2O$$

Moreover since the catalysts present in the process are sensitive to sulfur poisoning, a desulfurization step is placed upstream. It consists in converting sulfur compounds into gaseous hydrogen sulfide:

$$RS + H_2 \rightarrow H_2S + RH$$

Then hydrogen sulfide is converted into zinc sulfide by passing through zinc oxide:

$$H_2S + ZnO \rightarrow ZnS + H_2O$$

I.2.3.Sorption enhanced steam methane reforming

As seen before, two steps are required because of the thermodynamic limitation. A solution to overcome it is to use a sorption enhanced process. In the sorption enhanced water gas shift reaction, CO_2 is removed from the effluent by a sorbent such as CaO [9].

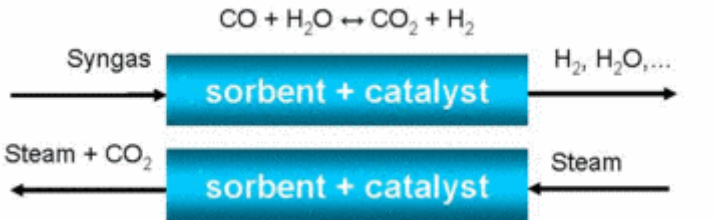

Figure 5: principle of the SEWGSR

The equilibrium is therefore shifted towards the production of hydrogen, increasing the conversion of CO. There are several benefits to use sorption enhanced water gas shift reaction, first of all the reaction can be performed in only one stage rather than two, a lower H_2O/CO ratio can be used and the temperature can be higher, improving the kinetics. Therefore the amount of catalyst for the water gas shift reaction, which usually represents the larger volume in the process, can be lower.

Membranes can also be used to remove one of the products by allowing a species to go through it and not the others, and they can also be a part of the catalytic active surface. In the case of H_2 permeation, hydrogen with high purity is produced. [10,11]. Pd membranes show good results compared to ceramic mesoporous membranes [12], microporous membranes are also studied.

Table 3
CO conversion for different membrane reactors (with the same dimensions) calculated by using the Temkin's reaction rate (theoretical results)[a]

Membrane reactor	CO conversion (%)
Palladium (thickness = 75×10^{-5} m)	83.93
Palladium (thickness = 75×10^{-6} m)	93.23
Mesoporous	82.26

[a] Mix1; $Q_{feed} = 4.56 \times 10^{-5}$ mol/s; $H_2O/CO = 1.1$; $T = 595$ K; $P_{lumen} = P_{shell} = 1$ atm; palladium membrane reactor: $Q_{sweep} = 43.6$ ml/min; mesoporous membrane reactor: no sweep gas.

Table 1: comparison of different membranes

I.2.4.Fuel cells

A PEM fuel cell (Proton Exchange Membrane fuel cell) is a promising device for power generation from hydrogen. It converts the chemical energy into electrical energy by reverse electrolysis. Hydrogen is dissociated on the anode into protons and electrons and the protons go through the membrane whereas the electrons are conducted in an external circuit. Oxygen then reacts with protons and electrons to form water on the cathode.

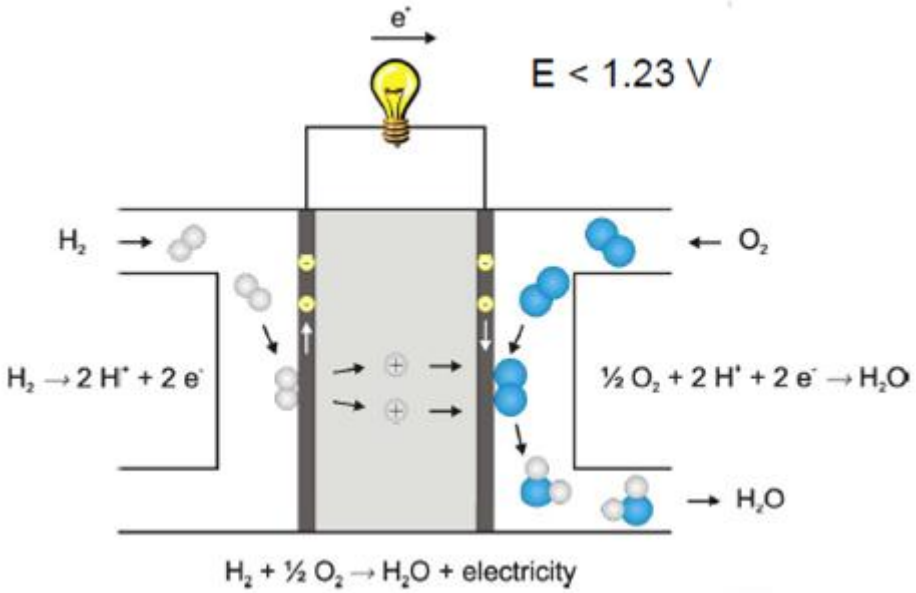

Figure 6: Principle of a hydrogen fuel cell

The purity of hydrogen is crucial for fuel cell applications since the Pt anode is highly contaminated by CO, as shown on Table 2 [13]:

Table 4
Hydrogen fuel quality specification: Current ISO and SAE directory for transportation hydrogen [136].

Species	Quantity limit
Helium	300 μmol/mol
Nitrogen and argon	100 μmol/mol
Water	5 μmol/mol
Carbon dioxide	2 μmol/mol
Oxygen	5 μmol/mol
Carbon monoxide	0.2 μmol/mol
Sulfur species	0.004 μmol/mol
Hydrocarbon species	2 μmol/mol
Ammonia	0.1 μmol/mol
Halogenated species	0.05 μmol/mol
Formaldehyde	0.01 μmol/mol
Formic acid	5 μmol/mol

Table 2: Hydrogen fuel quality specification for PEM fuel cells

The usual composition of the fuel resulting of methanol reforming is 74% H_2, 25%CO_2 and 1-2%CO [14]. The presence of high concentration of carbon dioxide can lead to reverse water gas shift reaction inside of the fuel cell, leading to a CO equilibrium concentration of 20-100ppm [15]

CO tolerant electrodes are investigated in order to overcome these difficulties [16, 17].

I.3.Kinetics and mechanism

I.3.1.Micro kinetic models

Two types of mechanisms have been highlighted in the literature: the redox mechanism and the associative mechanism.

Redox mechanism	Associative mechanism
CO + * ↔ CO*	CO + * ↔ CO*
H2O + * ↔ H2O*	H2O + * ↔ H2O*
H2O* + * ↔ OH* + H*	H2O* + * ↔ OH* + H*
OH* + * ↔ O* + H*	**CO* + OH* ↔ COOH* + ***
CO* + O* ↔ CO2* + *	**COOH* + * ↔ H* + CO2***
CO2* ↔ CO2 + *	CO2* ↔ CO2 + *
2H* ↔ H2 + 2*	2H* ↔ H2 + 2*

Table 3: Redox and associative mechanism. The different steps between the mechanisms are bold. * is a vacant site and X* is the adsorbed X species

It is accepted that the redox mechanism describes well the high temperature shift over ferrochrome catalysts, but there are still discussions about the mechanism of the low temperature shift, both redox and associative have been used in the literature. Some variations of these mechanisms have been proposed, including other elementary steps. For example, Callaghan et al. have developed a complex micro kinetic model for LTS over Cu(111) based on 17 elementary steps [18].

	$\vec{E}_j$	$\vec{A}_j$	Elementary reactions	$\overleftarrow{E}_j$	$\overleftarrow{A}_j$	ΔH	
s_1:	0	10^6	$H_2O + S \leftrightarrows H_2OS$	13.6	10^{14}	−13.6	a,b
s_2:	0	10^6	$CO + S \leftrightarrows COS$	12.0	10^{14}	−12.0	a,b
s_3:	5.3	4×10^{12}	$CO_2S \leftrightarrows CO_2 + S$	0	10^6	5.3	a,b
s_4:	15.3	10^{13}	$HS + HS \leftrightarrows H_2S + S$	12.8	10^{13}	2.5	a
s_5:	5.5	6×10^{12}	$H_2S \leftrightarrows H_2 + S$	0	10^6	5.5	a,b
s_6:	25.4	10^{13}	$H_2OS + S \leftrightarrows OHS + HS$	1.6	10^{13}	23.8	a
s_7:	10.7	10^{13}	$COS + OS \leftrightarrows CO_2S + S$	28.0	10^{13}	−17.3	a
s_8:	0	10^{13}	$COS + OHS \leftrightarrows HCOOS + S$	20.4	10^{13}	−20.4	a
s_9:	15.5	10^{13}	$OHS + S \leftrightarrows OS + HS$	20.7	10^{13}	−5.2	a
s_{10}:	0	10^{13}	$COS + OHS \leftrightarrows CO_2S + HS$	22.5	10^{13}	−22.5	a
s_{11}:	1.4	10^{13}	$HCOOS + S \leftrightarrows CO_2S + HS$	3.5	10^{13}	−2.1	a
s_{12}:	4.0	10^{13}	$HCOOS + OS \leftrightarrows CO_2S + OHS$	0.9	10^{13}	3.1	a
s_{13}:	29.0	10^{13}	$H_2OS + OS \leftrightarrows 2OHS$	0	10^{13}	29.0	a
s_{14}:	26.3	10^{13}	$H_2OS + HS \leftrightarrows OHS + H_2S$	0	10^{13}	26.3	a
s_{15}:	1.3	10^{13}	$OHS + HS \leftrightarrows OS + H_2S$	4.0	10^{13}	−2.7	a
s_{16}:	0.9	10^{13}	$HCOOS + OHS \leftrightarrows CO_2S + H_2OS$	26.8	10^{13}	−25.9	a
s_{17}:	14.6	10^{13}	$HCOOS + HS \leftrightarrows CO_2S + H_2S$	14.2	10^{13}	0.4	a

a—activation energies in kcal/mol ($\theta \to 0$ limit) estimated according to [1] and coinciding with the estimations made in [8]; pre-exponential factors from [2]. b—pre-exponential factors adjusted so as to fit the thermodynamics of the overall reaction; the units of the pre-exponential factors are $Pa^{-1}s^{-1}$ for adsorption/desorption reactions and s^{-1} for surface reactions.

Table 4: Microkinetic model for WGSR over Cu(111)

Moreover the intermediate in the associative mechanism is not well identified yet, some studies report that formate (HCOO) is the intermediate, but recent studies tend to prove that carboxyl is more probable.

I.3.2.Reaction orders

Several kinetic expressions have been published such as the Langmuir-Hinshelwood model, but the most useful expression to describe the kinetic law of the water gas shift reaction is the power law model:

$$r = kP_{CO}^{n_{CO}} P_{H_2O}^{n_{H_2O}} P_{CO_2}^{n_{CO_2}} P_{H_2}^{n_{H_2}} (1 - \beta)$$

With $\beta = \frac{P_{CO_2} P_{H_2}}{K P_{CO} P_{H_2O}}$, the approach to equilibrium

$k = k_0 exp\left(\frac{-Ea}{RT}\right)$, k_0 the pre exponential factor and Ea the activation energy

Many kinetic studies have been done to obtain reaction orders and activation energies for the water gas shift reaction over different catalysts and different conditions. Table 5 summarizes the most relevant results of the literature:

Catalyst	Temperature (°C)	Activation energy (kJ/mol)	Reaction order				Reference
			CO	H2O	CO2	H2	
8% CuO–Al2O3	200	62	0.9	0.8	-0.7	-0.8	[8]
8% CuO–15%CeO2–Al2O3	200	32	0.7	0.6	-0.6	-0.6	
8% CuO–CeO2	240	56	0.9	0.4	-0.6	-0.6	
40% CuO–ZnO–Al2O3	190	79	0.8	0.8	-0.9	-0.9	
Cu(111)	340	71	0	0.5–1	–	–	[19]
Cu(110)	340	42	0	1	–	–	[20]
1% Pt/CeO2	150–400	91 ± 5	0.14 ± 0.04	0.66 ± 0.14	-0.08 ± 0.03	-0.54 ± 0.03	[21]
1% Pt/TiO2	150–400	59 ± 3	0.30 ± 0.05	0.85 ± 0.10	-0.00 ± 0.03	-0.67 ± 0.03	
80-90%Fe2O3, 8-13% Cr2O3, 1-2%CuO	450	111	1	0	-0.36	-0.09	[22]
80-95%Fe2O3, 5-10% Cr2O3, 1-5%CuO	450	88	0.9	0.31	-0.156	-0.05	
1%Pt/ Al2O3	225-285	68	0.1	1.1	-0.07	-0.44	[23]
1%Pt/ Al2O3	285-345	84	0.06	1	-0.09	-0.44	
2%Pt/ Al2O3	270	82	0.21	0.75	-	-	
0.4%Pt/ Al2O3	544	39	0.45	0.37	0	-0.73	
Au/CeO2	180	40 ± 2	1	1	-0.5	-0.7	[24]

Table 5: Reaction orders and activation energy for different catalysts and conditions

It shows that the kinetic of the water gas shift reaction is complex, and the mechanism might be different depending on the type of catalyst, its composition or the temperature.

The reaction order of CO_2 is always found negative in these studies but it is not explained by most of the mechanisms, including the redox mechanism.

I.3.3.DFT calculations

The Density Functional Theory has been used by several authors to try to find the mechanism over different catalysts.

Gokhale et al. concluded that the redox mechanism plays no significant role on the water gas shift reaction over Cu(111). Moreover they proposed that formate is only a spectator species, resulting of the reaction between adsorbed CO_2 and H. This may explain the negative reaction order of CO_2, badly explained by most of the kinetic laws coming from these mechanisms [25].

DFT calculations were also used with copper and gold nanoparticles [26] The activity was found decreasing as follows: Cu_{29}>Cu(100)>Au_{29}>Au(100). They concluded that the redox mechanism is preferred on Cu(100) whereas the associative mechanism is preferred for the others. The water dissociation was nevertheless identified as the rate determining step for all of these catalysts.

Due to its sulfur tolerance, MoS_2 was also studied by DFT, with the conclusion that the reaction is through the redox mechanism, and that HCOO, formed by CO_2 and H, reacts further to form H_2COO and then CH_2O and O [27]. The effect of Co as a promoter on a Co-MoS_2 catalyst has been studied too. It was concluded that the redox mechanism was preferable compared to the associative mechanism, with the dissociation of OH into O and H. Formate is formed as an intermediate species. The effect of cobalt is to create more active sites and to increase the reaction rate [28].

I.3.4.Catalysts

Additionally to the industrial catalysts (ferrochrome and CuO/ZnO), other types of catalysts have been studied for different goals: improvement with promoters, better resistance to deactivation or to poisoning, better activity or selectivity.

I.3.4.1.High temperature shift catalysts

The typical composition of the ferrochrome catalyst is Fe_2O_3, about 10% Cr_2O_3 and CuO [22]. This catalyst is very active in the range of temperature of the HTS (310°C-450°C) but not at lower temperatures.

This catalyst needs to be activated before startup. The hematite is reduced to magnetite using the process gas. Cr_2O_3 is also reduced to CrO_3.

$$3Fe_2O_3 + H_2 \rightarrow 2Fe_3O_4 + H_2O$$

$$3Fe_2O_3 + CO \rightarrow 2Fe_3O_4 + CO_2$$

And:

$$2CrO_3 + 3H_2 \rightarrow Cr_2O_3 + H_2O$$

$$2CrO_3 + CO \rightarrow Cr_2O_3 + CO_2$$

This step is carefully controlled to avoid over-reduction that can cause damage to the catalyst pellets. Rhodes et al. (1995) proposed to control the reduction using a reduction factor for the reactor feed:

$$R = \frac{(CO) + (H_2)}{(CO_2) + (H_2O)}$$

This factor should be less than 1.2, and severe over-reduction is observed for R>1.6 [29].

Many studies have been carried out to improve the performances of the HTS catalyst. Diverse compositions of the ferrochrome catalyst have been tested, but different materials like noble metals were considered too.

I.3.4.1.1.Deactivation

Cr_2O_3 is used as a support to prevent sintering, which is the first cause of deactivation.

The second cause of deactivation after sintering is sulfur poisoning. It has been found that even at low concentrations (11-35 ppm), H_2S affects the reaction rate with a negative reaction order (-0.30) [30]. A desulphurization unit must therefore be placed before the water gas shift reactors. It is even

more important in the case of sorption enhanced water gas shift reaction because the membrane can also be poisoned by sulfur, or H_2S can be co-adsorbed with CO_2 by the sorbent.

I.3.4.1.2.Promoters

In order to improve the performances of the HTS catalyst, addition of promoters to FeCr have been analyzed. Catalysts containing 2% of different promoters have been tested by Rhodes et al., with the conclusion that the activity is changed according to Hg>Ag,Ba>Cu>Pb>unpromoted>B [31].

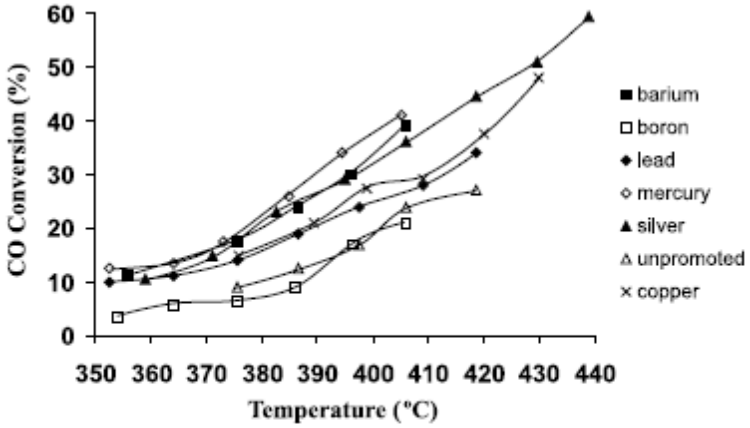

Figure 7: Effect of temperature on CO conversion on modified Fe_3O_4/Cr_2O_3 catalysts

The mechanism doesn't seem to change with the addition of copper, indicating that the active sites are similar [32].

Nanocrystalline ferrospinel structures have also been investigated, in order to study the role of Cu as a codopant for these materials (Fe:M with M=Cr, Ce, Ni, Co, Mn, Zn). It was concluded that copper plays a role in the conversion of hematite into magnetite, and into wustite in the case of cerium, which decrease the activity of the catalyst [33].

I.3.4.1.3.Cr-free catalysts

Chromium and more particularly its hexavalent form, is toxic for humans and environment. There have been some studies to propose HTS catalysts without Cr, especially for fuel cell applications. Aluminium, associated with copper, was found to be a good textural promoter for iron. Ga and Mn were also tested but showed poor results. [34].

Catalyst[a]	Surface area (m^2/g)		CO conversion (%)		
	Pre-reduction	Post-reduction	350 °C	400 °C	450 °C
Fe-only	19	12	8	20	27
Fe–Cr	54	43	19	43	56
Fe–Al	61	54	11	27	43
Fe–Ga	31	NA	NA	12	NA
Fe–Mn	64	NA	NA	16	NA
Equilibrium conversion			73	78	82

[a] Synthesis variables: Fe/Al (Cr, Ga, Mn = 10), pH 9, T_{cal} = 450 °C. Reduced at 350 °C with 20% H_2/N_2 for 2 h.

Table 6: BET surface measurements and % CO conversion over Fe-based catalysts with different textural promoters

Cu was the most effective promoter compared to Zn and Co in this FeAl catalyst, and the preparation method plays a significant role in the activity of the catalyst.

Table 6
BET surface area measurements and % CO conversion over Fe–Al catalysts: effect of structural promoters

Catalyst[a]	Surface area (m^2/g)	CO conversion (%)[b]
Fe–Al	61	25
Fe–Al–Zn (two-step)	78	19
Fe–Al–Co (two-step)	84	34
Fe–Al–Cu (two-step)	88	46

[a] Synthesis variables: Fe/Al (Cr, Ga, Mn = 10), Fe/Cu (Co, Zn) = 20, pH 9, T_{cal} = 450 °C.
[b] Reaction conditions: 400 °C, $CO/H_2O/N_2$ = 1/1/8, feed flow rate = 100 cm^3 (STP)/min, equal weight reactions (0.1 g), *in situ* reduction at 350 °C under 20% H_2/N_2 for 2 h.

Table 7: BET surface area measurements and % CO conversion over Fe-Al catalysts: affect of structural promoters

ZnFeNi and CoFeNi catalysts were investigated and 5%Zn/Fe/20%Ni and 5%Co/Fe/20%Ni revealed to be more active than a commercial FeCr catalyst [35].

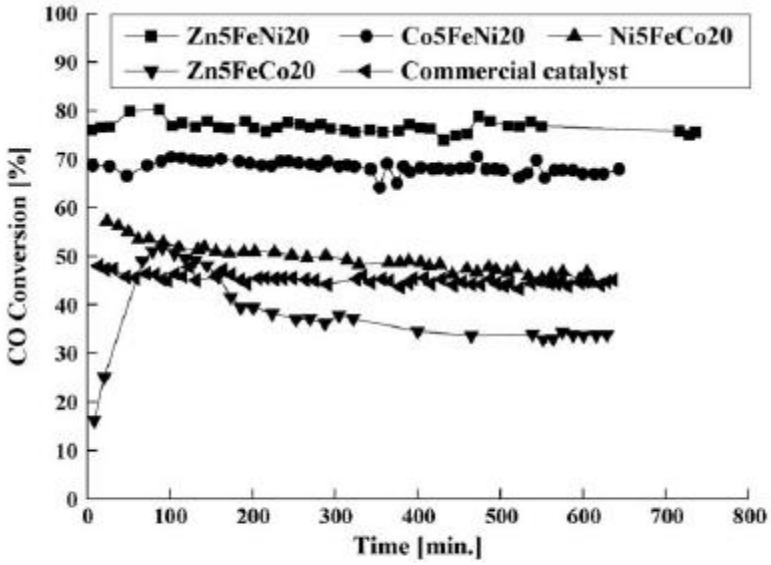

Figure 8: CO conversions of commercial and prepared three component catalysts at 400°C as a function of time

I.3.4.1.4.Ni-based catalysts

Ni based catalysts have been investigated recently as an alternative for the water gas shift reaction. This catalyst needs a pretreatment and is also active for methanation [36]. It has been shown that the impregnation of a Ni catalyst with K increases the activity and the selectivity with regards to the methanation, and prevents the carbon deposition [37].

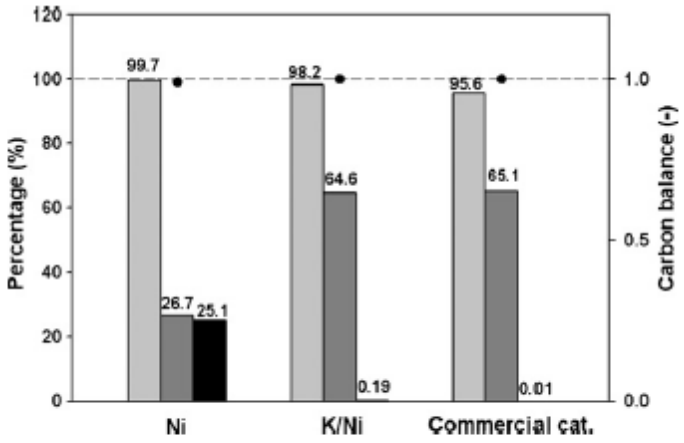

Figure 9: Comparison of three different catalysts for WGS reaction at 350°C and GHSV of 4000 h^{-1}. Gray bar: CO conversion (%); dark gray bar: H_2 production (%); black bar: CH_4 production; black dot: carbon balance (-)

The kinetics of the water gas shift reaction and of steam reforming and methanation over nickel have been studied by Xu and Froment [38]. They obtained thermodynamic values (activation energy, rate coefficient, enthalpy, adsorption constants…) for the three reactions. For the water gas shift reaction:

$$r = k\frac{P_{CO}P_{H_2O}P_{H_2}^{-1}(1-\frac{P_{CO_2}P_{H_2}}{KP_{CO}P_{H_2O}})}{(1+K_{CO}P_{CO}+K_{H_2}P_{H_2}+K_{CH_4}P_{CH_4}+K_{H_2O}\frac{P_{H_2O}}{P_{H_2}})}$$

With:

$$k = 1{,}955.10^6 \exp\left(\frac{67.13.10^3}{RT}\right) \qquad kg.kg_{cat}^{-1}.h^{-1}.bar^{-1}$$

I.3.4.2.Low temperature shift catalysts

CuO-ZnO was used in the early 1960's. Then Al_2O_3 was added as a support to reduce deactivation of the catalyst by sintering. CuO-ZnO/Al_2O_3 is the most used in the industry for the LTS, with 33%CuO, 34%ZnO, 33%Al_2O_3 as a typical composition. This catalyst is highly sensitive to sulphur poisoning, more than the ferrochrome catalyst.

The reduction of copper occurs during the startup:

$$CuO + H_2 \rightarrow Cu + H_2O$$

I.3.4.2.1.Deactivation

The first cause of deactivation of the LTS catalyst is sintering. Indeed, copper has a low melting temperature and sintering occurs if the catalyst is heated above 300°C.

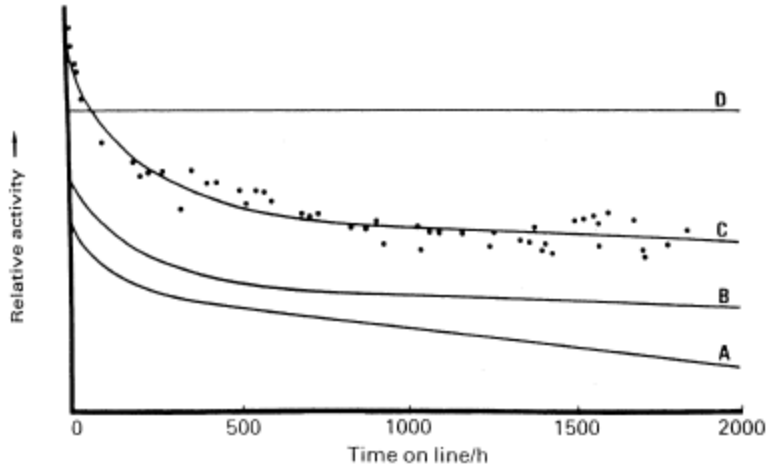

Fig. 1. Relative activities of typical copper/zinc oxide low-temperature water-gas shift catalysts under poison-free conditions. (A) Cr_2O_3-based catalyst; (B) conventional Al_2O_3-based catalyst; (C) high copper-content Al_2O_3-based catalyst; (D) optimised Al_2O_3-based catalyst. For clarity, experimental points are shown on only one of the curves.

Figure 10: Deactivation of low temperature catalysts

The second cause of deactivation is sulfur poisoning. To avoid rapid deactivation by sulfur, concentration of S must be below 0.1ppm. The reaction is:

$$2Cu + H_2S \rightarrow Cu_2S + H_2 \qquad \Delta H^0 = -59.4\ kJ/mol$$

ZnO helps to limit sulfur poisoning by absorption of H_2S:

$$ZnO + H_2S \rightarrow ZnS + H_2O \qquad \Delta H^0 = -76.7\ kJ/mol$$

Its equilibrium constant at 500K is $7.4.10^7$, so the reaction is favored thermodynamically.

Chlorides are also a problem for this catalyst by accelerating the sintering because of the formation of compounds with low melting point [39]:

$$Cu + HCl \rightarrow CuCl + \frac{1}{2}H_2 \qquad \Delta H^0 = -43.5\ kJ/mol$$

$$ZnO + 2HCl \rightarrow ZnCl_2 + H_2O \qquad \Delta H^0 = -121.8\ kJ/mol$$

I.3.4.2.2.Ceria-based catalysts

Ceria is a component of the three way catalyst for cars, one of its function is the WGS activity. A series of ceria-supported catalysts have been tested, and it was found that the activity decreased as: $CuO/ZnO/Al_2O_3$>Pd/Ce,Ni/Ce>Fe/Ce,Co/Ce>CeO_2>Pd/silica [40].

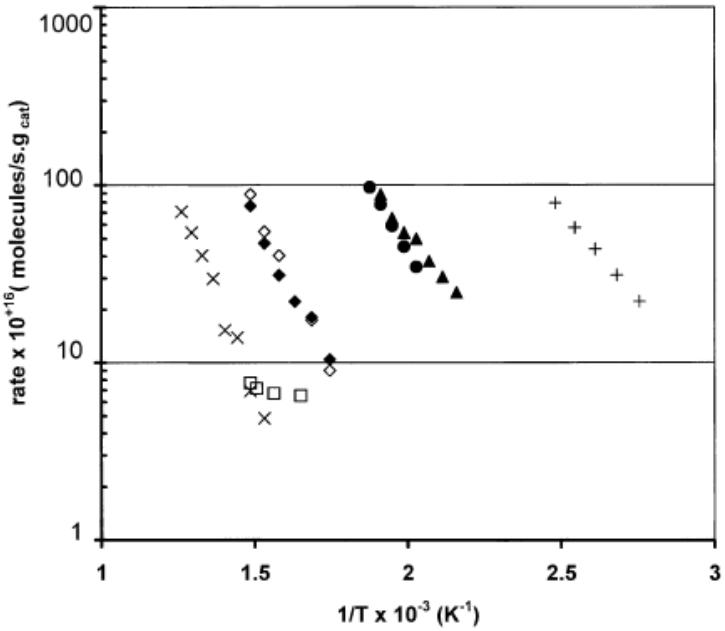

Fig. 1. Differential rates for the water-gas-shift reaction on various catalysts using partial pressures of 24 and 22 Torr for CO and H_2O, respectively. Data are shown for the following catalysts: (+) Cu/ZnO/alumina; (▲) Pd/CeO_2; (●) Ni/CeO_2; (◇) Co/CeO_2; (◆) Fe/CeO_2; (□), Pd/SiO_2; and (×) CeO_2.

Figure 11: comparison of different Ce-based catalysts

It was also concluded that the redox mechanism represents well the kinetics of the water gas shift reaction over Ce. Cu and Ni improve the activity of $Ce(La)O_x$ catalyst. Cu-Ce keeps its high activity and stability at high temperature and requires no activation before use [41].

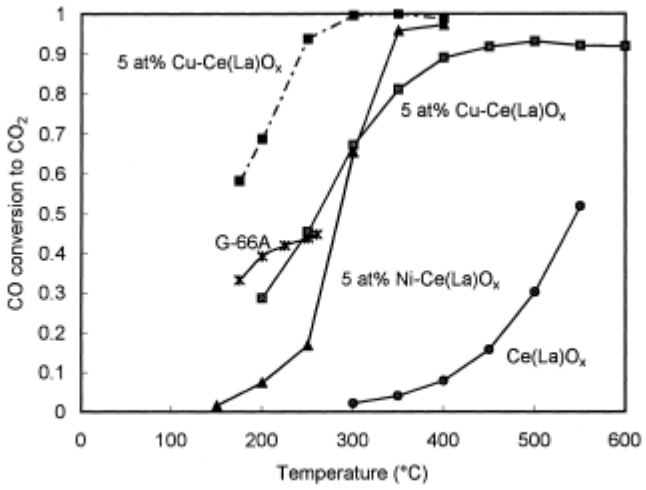

Figure 12: WGS reactivity over ceria-based catalysts, 2%CO, 10.7%H_2O, He; Solid lines SV=80000/h;Dashed line SV=8000/h

I.3.4.3.Noble metals

Noble metals have been tested for this reaction by Grenoble et al. [42]. Among them, it may be noted that Pt and Au are the most promising catalysts, especially for fuel cells since these materials are non pyrophoric and do not need pretreatment before use.

I.3.4.3.1.Platinum based catalysts

Platinum catalysts are known to be very active for the water gas shift reaction but were not studied because they are expensive. The possible use in fuel cell has however led to a renewed interest for noble metals catalysts, especially for platinum.

The redox mechanism has been proposed for Pt-Al_2O_3 and Pt/CeO_2 [23, 43], but dual-site mechanism may be better to take into account the effect of the support [21]:

$$CO + * \rightleftarrows CO^* \quad (1)$$

$$H_2O + O{-}S \rightleftarrows HO{-}S{-}OH \quad (2)$$

$$CO^* + HO{-}S{-}OH \rightleftarrows COOH^* + S{-}OH \quad (3)$$

$$COOH^* + S{-}OH + * \rightarrow 2H^* + S{-}O{-}CO_2 \quad (4)$$

$$2H^* \rightleftarrows H_2 + 2^* \quad (5)$$

$$S{-}O{-}CO_2 \rightleftarrows CO_2 + S{-}O \quad (6)$$

* is a metallic site and S–O is an adsorption site on the support.

The water gas shift reaction has been tested over Pt-based catalysts deposited on different surfaces. Among several supports, ceria and titanium are the most promising materials. Enhancement of these supports has been studied: the Pt/CeO_2 catalyst can be improved by addition of zirconia, Pt/ZrO_2 is itself not really active for the water gas shift reaction [43].

Table 3
Results of water–gas shift activity tests carried out in a fixed bed reactor, in the presence of H_2 and CO_2

Temperature (°C)	225	250	275	300
Catalyst description	CO conversion (%)			
1% Pt/CeO_2	13.8	26	43.3	61.3
1% Pt/$Ce_{0.90}Zr_{0.10}O_2$	13.7	33.9	57.4	70.9
1% Pt/$Ce_{0.75}Zr_{0.25}O_2$	16.2	39.3	54.3	67.9
1% Pt/$Ce_{0.50}Zr_{0.50}O_2$	16.7	41.3	58.5	73.6
1% Pt/$Ce_{0.25}Zr_{0.75}O_2$	17.5	33.3	47.1	64.3
1% Pt/ZrO_2	7	16.5	26.9	42.7
Thermodynamic equilibrium conversion limit	95.2	92.2	88.1	82.7

Conditions: H_2O:CO:H_2:CO_2:N_2 = 26.1:3.0:29.8:11.2:29.9%. Total gas flow = 250 cm^3/min.

Table 8: Comparison of Pt-based catalysts

Pt/Ce-TiO_2 shows a good activity and is moreover is stable at high temperature whereas Pt/TiO_2 is not [44].

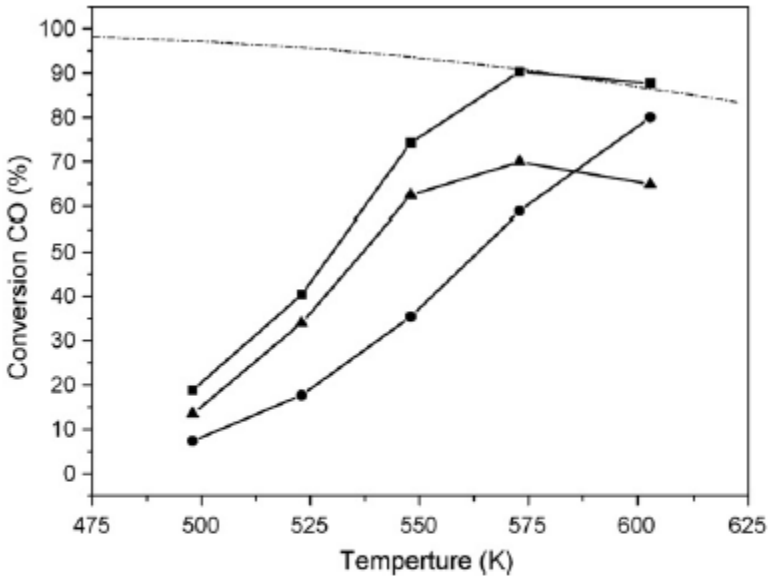

Figure 13: Comparison between (●)Pt/CeO_2, (▲)Pt/TiO_2, (■) Pt/Ce-TiO_2. Dotted line shows the thermodynamic equilibrium

I.3.4.3.2.Gold catalysts

Gold catalysts have been studied at low temperature using DFT and X-ray absorption spectroscopy. The activity of different Au-based catalysts can be compared: Au(111) has a low activity compared to the other low temperature catalyst, especially to Cu (100). Gold has a better activity when associated to metal oxides such as CeO_2, ZnO [45], TiO_2 [46] or MoO_2 [47]. Among these catalysts, Au/ZnO is not as active as the industrial catalyst Cu/ZnO but the others have a similar activity. Moreover the coupling of CeO_2 and TiO_2 appeared to be very active [48].

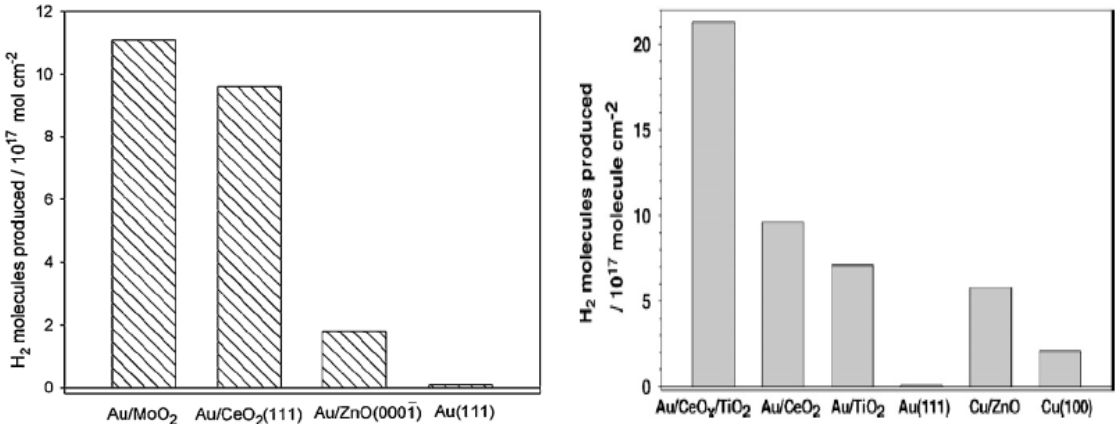

Figures 14: Comparison between Au-supported catalysts and Cu catalysts

I.4.Methanation

Methanation needs to be studied because it occurs in the same time as the water gas shift reaction, especially on nickel catalysts [36,37]. Its conversion is low but it has an influence on the mass balances, moreover the kinetics of this reaction could be discussed as well from the results of the experiments.

A microkinetic model has been proposed by Alstrup [50]. Alstrup neglected the formation of CO_2, considering only the formation of H_2O:

(1) $CO + * \leftrightarrow CO*$
(2) $H_2 + 2* \leftrightarrow H_2*$
(3) $CO* + * \leftrightarrow C* + O*$
(4) $C* + H* \leftrightarrow CH* + *$
(5) $CH* + H* \leftrightarrow CH_2* + *$
(6) $CH_2* + H* \leftrightarrow CH_3* + *$
(7) $CH_3* + H* \rightarrow CH_4 + 2*$
(8) $O* + H* \rightarrow OH* + *$
(9) $OH* + H* \rightarrow H_2O* + *$

Good agreement with experiments was found by considering hydrogenation of CH* (step 7) as the rate determining step.

However the direct dissociation of CO on Fe and Co catalysts has been found to be a minor contributor to the CH formation [51]. A H-assisted dissociation, with formation of formyl and hydroxymethylene intermediates and CO_2 as a product, was then proposed:

(1) $CO + * \leftrightarrow CO*$
(2) $H_2 + 2* \leftrightarrow H_2*$
(6) $CO* + H* \leftrightarrow HCO* + *$
(7) $HCO* + H* \leftrightarrow HCOH* + *$
(8) $HCOH* + * \leftrightarrow CH* + OH*$
(9) $OH* + H* \leftrightarrow H_2O* + *$
(10) $CH* + H* \leftrightarrow CH_2* + *$
(11) $CH_2* + H* \leftrightarrow CH_3* + *$
(12) $CH_3* + H* \leftrightarrow CH_4 + 2*$

II.Langmuir-Hinshelwood model

In addition to the traditional redox and associative mechanisms, mechanisms involving COH as an intermediate species were investigated. The rate expressions were obtained based on one rate determining step and the others at equilibrium.

For all the following expressions, k_i is the rate constant of the step (i), $K_i = \frac{k_i}{k_{-i}}$ and $\beta = \frac{P_{CO_2} P_{H_2}}{K P_{CO} P_{H_2O}}$.

II.1.Redox mechanism

(1) CO + * ↔ CO*
(2) H_2O + * ↔ H_2O*
(3) H_2O* + * ↔ OH* + H*
(4) OH* + * ↔ O* + H*
(5) CO* + O* ↔ CO_2* + *
(6) CO_2* ↔ CO_2 + *
(7) 2H* ↔ H_2 + 2*

If step 3 (water dissociation) is the rate determining step:

$$r_3 = \frac{k_3 K_2 P_{H_2O}(1-\beta)}{(1 + K_1 P_{CO} + K_2 P_{H_2O} + \frac{P_{CO_2}}{K_6} + \sqrt{\frac{P_{H_2}}{K_7}} + \frac{1}{K_1 K_5 K_6}\frac{P_{CO_2}}{P_{CO}} + \frac{1}{K_1 K_4 K_5 K_6 \sqrt{K_7}}\frac{P_{CO_2}\sqrt{P_{H_2}}}{P_{CO}})^2}$$

If step 4 (OH dissociation) is the rate determining step:

$$r_4 = \frac{k_4 K_2 K_3 \sqrt{K_7} P_{H_2O} P_{H_2}^{-0.5}(1-\beta)}{(1 + K_1 P_{CO} + K_2 P_{H_2O} + \frac{P_{CO_2}}{K_6} + \sqrt{\frac{P_{H_2}}{K_7}} + \frac{1}{K_1 K_5 K_6}\frac{P_{CO_2}}{P_{CO}} + K_2 K_3 \sqrt{K_7}\frac{P_{H_2O}}{\sqrt{P_{H_2}}})^2}$$

If step 5 (CO_2 formation) is the rate determining step:

$$r_5 = \frac{\frac{k_5}{K_5 K_6} P_{CO} P_{H_2O} P_{H_2}^{-1}(1-\beta)}{(1 + K_1 P_{CO} + K_2 P_{H_2O} + \frac{P_{CO_2}}{K_6} + \sqrt{\frac{P_{H_2}}{K_7}} + K_2 K_3 K_4 K_7 \frac{P_{H_2O}}{P_{H_2}} + K_2 K_3 \sqrt{K_7}\frac{P_{H_2O}}{\sqrt{P_{H_2}}})^2}$$

II.2.Carboxyl mechanism

(1) CO + * ↔ CO*
(2) H_2O + * ↔ H_2O*
(3) H_2O* + * ↔ OH* + H*
(4') CO* + OH* ↔ COOH* + *
(5') COOH* + * ↔ H* + CO_2*
(6) CO_2* ↔ CO_2 + *
(7) 2H* ↔ H_2 + 2*

If step 3 (water dissociation) is the rate determining step:

$$r_3 = \frac{k_3 K_2 P_{H_2O}(1-\beta)}{(1 + K_1 P_{CO} + K_2 P_{H_2O} + \frac{P_{CO_2}}{K_6} + \sqrt{\frac{P_{H_2}}{K_7}} + \frac{1}{K_5 K_6 \sqrt{K_7}} P_{CO_2}\sqrt{P_{H_2}} + \frac{1}{K_1 K_4 K_5 K_6 \sqrt{K_7}} \frac{P_{CO_2}\sqrt{P_{H_2}}}{P_{CO}})^2}$$

If step 4' (COOH formation) is the rate determining step:

$$r_{4'} = \frac{k_4 K_1 K_2 K_3 \sqrt{K_7} P_{CO} P_{H_2O} P_{H_2}^{-0.5}(1-\beta)}{(1 + K_1 P_{CO} + K_2 P_{H_2O} + \frac{P_{CO_2}}{K_6} + \sqrt{\frac{P_{H_2}}{K_7}} + \frac{1}{K_5 K_6 \sqrt{K_7}} P_{CO_2}\sqrt{P_{H_2}} + K_2 K_3 \sqrt{K_7} \frac{P_{H_2O}}{\sqrt{P_{H_2}}})^2}$$

If step 5' (COOH dissociation) is the rate determining step:

$$r_{5'} = \frac{k_5 K_1 K_2 K_3 K_6 \sqrt{K_7} P_{CO} P_{H_2O} P_{H_2}^{-0.5}(1-\beta)}{(1 + K_1 P_{CO} + K_2 P_{H_2O} + \frac{P_{CO_2}}{K_6} + \sqrt{\frac{P_{H_2}}{K_7}} + K_1 K_2 K_3 K_6 \sqrt{K_7} \frac{P_{H_2O} P_{CO}}{\sqrt{P_{H_2}}} + K_2 K_3 \sqrt{K_7} \frac{P_{H_2O}}{\sqrt{P_{H_2}}})^2}$$

II.3.Mechanism involving COH

(1) CO + * ↔ CO*
(2) H_2O + * ↔ H_2O*
(3) H_2O* + * ↔ OH* + H*
(4) OH* + * ↔ O* + H*
(α) CO* + H* ↔ COH* + *
(β) COH* + O* ↔ COOH* + *
(γ) COOH* + * ↔ H* + CO_2*
(6) CO_2* ↔ CO_2 + *
(7) 2H* ↔ H_2 + 2*

If step 4 (OH dissociation) is the rate determining step:

$$r_4 = \frac{k_4 K_2 K_3 \sqrt{K_7} P_{H_2O} P_{H_2}^{-0.5}(1-\beta)}{(1 + K_1 P_{CO} + K_2 P_{H_2O} + \frac{P_{CO_2}}{K_6} + \sqrt{\frac{P_{H_2}}{K_7}} + \frac{1}{K_1 K_6 K_\beta K_\gamma K_\alpha} \frac{P_{CO_2}}{P_{CO}} + K_2 K_3 \sqrt{K_7} \frac{P_{H_2O}}{\sqrt{P_{H_2}}} + \frac{K_1 K_\alpha}{\sqrt{K_7}} P_{CO}\sqrt{P_{H_2}} + \frac{1}{K_6 K_\alpha \sqrt{K_7}} P_{CO_2}\sqrt{P_{H_2}})^2}$$

If step α (COH formation) is the rate determining step:

$$r_\alpha = \frac{k_\alpha \frac{K_1}{\sqrt{K_7}} P_{CO} P_{H_2}^{0.5}(1-\beta)}{(1 + K_1 P_{CO} + K_2 P_{H_2O} + \frac{P_{CO_2}}{K_6} + \sqrt{\frac{P_{H_2}}{K_7}} + K_2 K_3 K_7 K_4 \frac{P_{H_2O}}{P_{H_2}} + K_2 K_3 \sqrt{K_7} \frac{P_{H_2O}}{\sqrt{P_{H_2}}} + \frac{1}{K_2 K_3 K_6 K_7 \sqrt{K_7} K_4 K_\gamma K_\beta} \frac{P_{CO_2} P_{H_2}\sqrt{P_{H_2}}}{P_{H_2O}} + \frac{1}{K_6 K_\alpha \sqrt{K_7}} P_{CO_2}\sqrt{P_{H_2}})^2}$$

If step β (COOH formation) is the rate determining step:

$$r_\beta = \frac{k_\beta K_1 K_2 K_3 K_\alpha K_4 \sqrt{K_7} P_{CO} P_{H_2O} P_{H_2}^{-0.5}(1-\beta)}{(1 + K_1 P_{CO} + K_2 P_{H_2O} + \frac{P_{CO_2}}{K_6} + \sqrt{\frac{P_{H_2}}{K_7}} + K_2 K_3 K_7 K_4 \frac{P_{H_2O}}{P_{H_2}} + K_2 K_3 \sqrt{K_7} \frac{P_{H_2O}}{\sqrt{P_{H_2}}} + \frac{K_1 K_\alpha}{\sqrt{K_7}} P_{CO}\sqrt{P_{H_2}} + \frac{1}{K_6 K_\alpha \sqrt{K_7}} P_{CO_2}\sqrt{P_{H_2}})^2}$$

If step γ (COOH dissociation) is the rate determining step:

$$r_\gamma = \frac{k_\gamma K_1 K_2 K_3 K_\beta K_\alpha \sqrt{K_7} P_{CO} P_{H_2O} P_{H_2}^{-0.5} (1-\beta)}{(1 + K_1 P_{CO} + K_2 P_{H_2O} + \frac{P_{CO_2}}{K_6} + \sqrt{\frac{P_{H_2}}{K_7}} + K_2 K_3 K_7 K_\alpha \frac{P_{H_2O}}{P_{H_2}} + K_2 K_3 \sqrt{K_7} \frac{P_{H_2O}}{\sqrt{P_{H_2}}} + \frac{K_1 K_\alpha}{\sqrt{K_7}} P_{CO} \sqrt{P_{H_2}} + K_1 K_2 K_3 K_\beta K_\alpha \sqrt{K_7} P_{CO} P_{H_2O} \sqrt{P_{H_2}})^2}$$

II.4.Mechanism involving COH and HCOOH

(1) CO + * ↔ CO*
(2) H_2O + * ↔ H_2O*
(3) H_2O* + * ↔ OH* + H*
(α') CO* + H* ↔ COH* + *
(β') COH* + OH* ↔ HCOOH* + *
(γ') HCOOH* + 2* ↔ CO_2* + 2H*
(6) CO_2* ↔ CO_2 + *
(7) 2H* ↔ H_2 + 2*

If step α' (COH formation) is the rate determining step:

$$r_{\alpha'} = \frac{k_\alpha \frac{K_1}{\sqrt{K_7}} P_{CO} P_{H_2}^{0.5} (1-\beta)}{(1 + K_1 P_{CO} + K_2 P_{H_2O} + \frac{P_{CO_2}}{K_6} + \sqrt{\frac{P_{H_2}}{K_7}} + K_2 K_3 \sqrt{K_7} \frac{P_{H_2O}}{\sqrt{P_{H_2}}} + \frac{1}{K_6 K_7 K_\gamma} P_{CO_2} P_{H_2} + \frac{1}{K_2 K_3 K_7 \sqrt{K_7} K_\beta K_\gamma} \frac{P_{CO_2} P_{H_2} \sqrt{P_{H_2}}}{P_{H_2O}})^2}$$

If step β' (HCOOH formation) is the rate determining step:

$$r_{\beta'} = \frac{k_\beta K_1 K_2 K_3 K_\alpha P_{CO} P_{H_2O} (1-\beta)}{(1 + K_1 P_{CO} + K_2 P_{H_2O} + \frac{P_{CO_2}}{K_6} + \sqrt{\frac{P_{H_2}}{K_7}} + K_2 K_3 \sqrt{K_7} \frac{P_{H_2O}}{\sqrt{P_{H_2}}} + \frac{1}{K_6 K_7 K_\gamma} P_{CO_2} P_{H_2} + \frac{K_1 K_\alpha}{\sqrt{K_7}} P_{CO} \sqrt{P_{H_2}})^2}$$

If step γ' (HCOOH dissociation) is the rate determining step:

$$r_{\gamma'} = \frac{k_\gamma K_1 K_2 K_3 K_\alpha K_\beta \sqrt{K_7} P_{CO} P_{H_2O} (1-\beta)}{(1 + K_1 P_{CO} + K_2 P_{H_2O} + \frac{P_{CO_2}}{K_6} + \sqrt{\frac{P_{H_2}}{K_7}} + K_2 K_3 \sqrt{K_7} \frac{P_{H_2O}}{\sqrt{P_{H_2}}} + K_1 K_2 K_3 K_\beta K_\alpha P_{CO} P_{H_2O} + \frac{K_1 K_\alpha}{\sqrt{K_7}} P_{CO} \sqrt{P_{H_2}})^2}$$

II.5.Summary

Redox mechanism	Associative mechanism
(1) CO + * ↔ CO*	(1) CO + * ↔ CO*
(2) H2O + * ↔ H2O*	(2) H2O + * ↔ H2O*
(3) H2O* + * ↔ OH* + H*	(3) H2O* + * ↔ OH* + H*
(4) OH* + * ↔ O* + H*	**(4') CO* + OH* ↔ COOH* + ***
(5) CO* + O* ↔ CO2* + *	**(5') COOH* + * ↔ H* + CO2***
(6) CO2* ↔ CO2 + *	(6) CO2* ↔ CO2 + *
(7) 2H* ↔ H2 + 2*	(7) 2H* ↔ H2 + 2*

rds	CO order	H2O order	CO2 order	H2 order
(3)	0	1	0	0
(4)	0	1	0	-0,5
(5)	1	1	0	-1
(4')	1	1	0	-0,5
(5')	1	1	0	-0,5

Table 9: Theoretical reaction orders

rds	CO order	H2O order	CO2 order	H2 order
(α)	0	1	0	-0.5
(β)	1	0	0	0.5
(γ)	1	1	0	-0.5
(δ)	1	1	0	-0.5
(α')	1	0	0	0.5
(β')	1	1	0	0
(γ')	1	1	0	0

Table 10: Theoretical reaction orders for the mechanisms involving COH

II.6.Methanation

The mechanism is divided into two possible pathways containing either the direct dissociation of CO or the H-assisted dissociation, as proposed by Iglesia et al. [51].

II.6.1.Unassisted CO dissociation

(1) $H_2 + 2^* \leftrightarrow H_2^*$
(2) $CO + * \leftrightarrow CO^*$
(3) $CO^* + * \leftrightarrow C^* + O^*$
(4) $C^* + H^* \leftrightarrow CH^* + *$
(5) $CO^* + O^* \leftrightarrow CO_2 + 2^*$
(10) $CH^* + H^* \leftrightarrow CH_2^* + *$
(11) $CH_2^* + H^* \leftrightarrow CH_3^* + *$
(12) $CH_3^* + H^* \leftrightarrow CH_4 + 2^*$

The reaction rate can be calculated assuming a rate determining step:

rds	Rate
(10)	$r = k_{app} P_{CO}^2 P_{H_2} P_{CO_2}^{-1} \left(1 - \frac{P_{CH_4} P_{CO_2}}{K \; P_{CO}^2 P_{H_2}^2}\right)$
(3)	$r = k_{app} P_{CO} \left(1 - \frac{P_{CH_4} P_{CO_2}}{K \; P_{CO}^2 P_{H_2}^2}\right)$
(4)	$r = k_{app} P_{CO}^2 P_{H_2}^{0,5} P_{CO_2}^{-1} \left(1 - \frac{P_{CH_4} P_{CO_2}}{K \; P_{CO}^2 P_{H_2}^2}\right)$
(5)	$r = k_{app} P_{CO}^2 P_{H_2}^2 P_{CH_4}^{-1} \left(1 - \frac{P_{CH_4} P_{CO_2}}{K \; P_{CO}^2 P_{H_2}^2}\right)$

II.6.2.H-assisted CO dissociation

(1) $CO + * \leftrightarrow CO*$
(2) $H_2 + 2* \leftrightarrow H_2*$
(6) $CO* + H* \leftrightarrow HCO* + *$
(7) $HCO* + H* \leftrightarrow HCOH* + *$
(8) $HCOH* + * \leftrightarrow CH* + OH*$
(9) $OH* + H* \leftrightarrow H_2O* + *$
(10) $CH* + H* \leftrightarrow CH_2* + *$
(11) $CH_2* + H* \leftrightarrow CH_3* + *$
(12) $CH_3* + H* \leftrightarrow CH_4 + 2*$

The reaction rate can be calculated assuming a rate determining step:

rds	Rate
(10)	$r = k_{app} P_{CO} P_{H_2O}^{-1} P_{H_2}^{2} \left(1 - \frac{P_{CH_4} P_{H_2O}}{K \; P_{CO} P_{H_2}^{3}}\right)$
(6)	$r = k_{app} P_{CO} P_{H_2}^{0,5} \left(1 - \frac{P_{CH_4} P_{H_2O}}{K \; P_{CO} P_{H_2}^{3}}\right)$
(7)	$r = k_{app} P_{CO} P_{H_2} \left(1 - \frac{P_{CH_4} P_{H_2O}}{K \; P_{CO} P_{H_2}^{3}}\right)$
(8)	$r = k_{app} P_{CO} P_{H_2} \left(1 - \frac{P_{CH_4} P_{H_2O}}{K \; P_{CO} P_{H_2}^{3}}\right)$

Except for (7) and (8), the reaction rates can be differentiated by the effect of the partial pressures of the species.

III.Experimental

III.1.Description of the setup

A diagram of the setup is shown in Figure 15. The reaction was run in a tubular packed bed reactor.

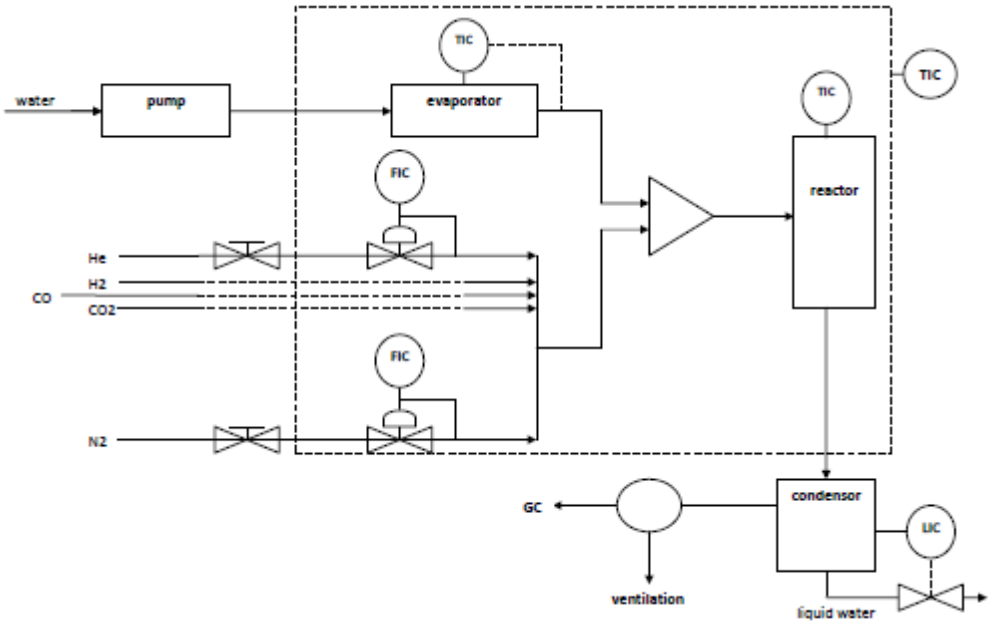

Figure 15: Schematic diagram of the setup

Three tubular packed-bed reactors have been used: steel (9mm ID, mm length), quartz (16mm ID, mm length), quartz (8mm ID, mm length). Only the last one was used for kinetic studies due to gas phase reaction into the others, as seen on Table 11.

	T °C	CO %	H_2O %	H_2 %	He %	total flow (mL/min)	Xeq %	X %
Steel reactor	500	6,1	50,9	0,0	43,0	244	97,4	5,5
Quartz reactor (16mm ID)	500	7,9	39,5	0,0	52,6	190	95,4	6,7
Quartz reactor (8mm ID)	400	5,0	15,0	2,5	77,5	400	94,4	0,07
	400	8,0	24,0	4,0	64,0	250	94,4	0,08
	450	5,0	15,0	2,5	77,5	400	91,6	0,10
	450	8,0	24,0	4,0	64,0	250	91,6	0,01
	500	5,0	15,0	2,5	77,5	400	88,3	0,11
	500	8,0	24,0	4,0	64,0	250	88,3	0,06

Table 11: Blank tests

The thermal mass flow controllers (EL-flow, Bronkhorst High-Tech) have been calibrated using a soap bubble flow meter. The steam is supplied by a pump (Model 501 solvent delivery system, Analytical Scientific Instruments, inc) followed by an evaporator. The other gases come from bottles (Yara Praxair).

	CO	H_2	CO_2
Minimum flowrate	6 mL/min	5 mL/min	2 mL/min

Table 12: Minimum flowrate for the gases

The products were analyzed by a gas chromatography (Agilent 3000 microGC) at the output of the reactor. The calibration has been made with gases with a known amount of the reactants and the products. To avoid small particles and water to go to the GC, a filter and a cold trap have been placed before it.

III.2.Catalyst samples

All the catalysts were prepared by co-precipitation. They were characterized by BET and by chemisorption.

	BET surface area (m^2/g_{cat})	dispersion (%)	Ni surface area (m^2/g_{cat})	Ni partical size (nm)
40%Ni	153	10.8	28	9

Table 13: Characteristic of the catalyst

The metal nitrates were diluted in an aqueous solution. A sodium solution was slowly added (about 3mL/min) and then the solution was placed in an oil bath for 16h at 80°C. The solid was filtered and dried either in an oven or by spray drying. Finally the samples were calcined at 600°C for 7 hours.

Before use, the catalyst was crushed and sieved to the desired particle size and was reduced overnight in the reactor under 25% of hydrogen with helium at 600°C.

III.3.Procedures

A small amount of catalyst (around 5mg) was placed in the reactor. The syngas composition was chosen after running some tests in order to reach a conversion between 5% and 25%. The ratio $\frac{H_2O}{CO}$ must be superior or equal to 3 in order to minimize the carbon deposition and the methanation.

During the measurements, methanation was observed. To take it into account, both the conversion of CO into CO_2 and into methane have been calculated by the following expressions:

$$X_{WGS} = \frac{moles\ of\ CO_2\ produced}{moles\ of\ CO\ fed};\ X_{methanation} = \frac{moles\ of\ CH_4\ produced}{moles\ of\ CO\ fed}.$$

The reactions are:

$$CO + H_2O \rightarrow H_2 + CO_2$$

$$2CO + 2H_2 \rightarrow CH_4 + CO_2$$

Here are the equations used to calculate the conversions:

$$F_{tot}^{out} = \frac{F_{CO}^{in} + F_{CO_2}^{in}}{x_{CH_4}^{out} + x_{CO}^{out} + x_{CO_2}^{out}}$$

$$X_{methanation} = \frac{x_{CH_4}^{out} + x_{CH_4}^{out}\frac{F_{CO_2}^{in}}{F_{CO}^{in}}}{x_{CH_4}^{out} + x_{CO}^{out} + x_{CO_2}^{out}}$$

$$X_{WGS} = \frac{-x_{CH_4}^{out} + x_{CO_2}^{out} - x_{CO}^{out}\frac{F_{CO_2}^{in}}{F_{CO}^{in}} - 2x_{CH_4}^{out}\frac{F_{CO_2}^{in}}{F_{CO}^{in}}}{x_{CH_4}^{out} + x_{CO}^{out} + x_{CO_2}^{out}}$$

$F_{CO_2}^{in}$ represents the flowrate of the component i in the inlet

F_{tot}^{out} represents the total dry flowrate

x_i^{out} represents the fraction of the component i in the dry outlet

The reaction rate is, for an integral reactor: $r = \frac{dX_{WGS}}{d\left(\frac{W}{F_{CO}^{i}}\right)}$, with W the weight of the catalyst. By working at low conversion of CO (>25%), the reaction rate is reduced to: $r = \frac{F_{CO}^{i} X_{CO}}{W}$.

The outlet of the reactor must not be at thermodynamic equilibrium. This was confirmed by calculating $\beta = \frac{P_{CO_2} P_{H_2}}{K \ P_{CO} P_{H_2O}}$. It must be under 0.2.

IV.Results and discussion

IV.1.Diffusion testing

In order to have correct results, there must be no mass and heat transport limitations. The diffusion problems are internal and external. The qualitative evolution of the concentration and the temperature is shown on Figure 16:

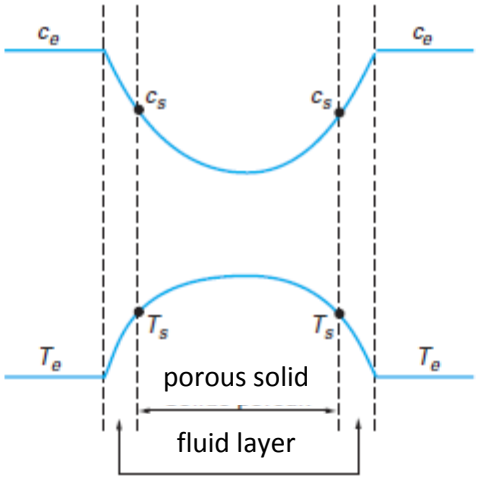

Figure 16: internal and external gradients of concentration and temperature

The diffusion depends on the flowrate, the size and the shape of the particles.

IV.1.1.Internal diffusion

The internal transfer was studied by using four different size distributions ($500\mu m<d_1<250\mu m<d_2<150\mu m<d_3<75\mu m<d_4$) under the same conditions. The curve CO conversion vs particle size is shown on Figure 17.

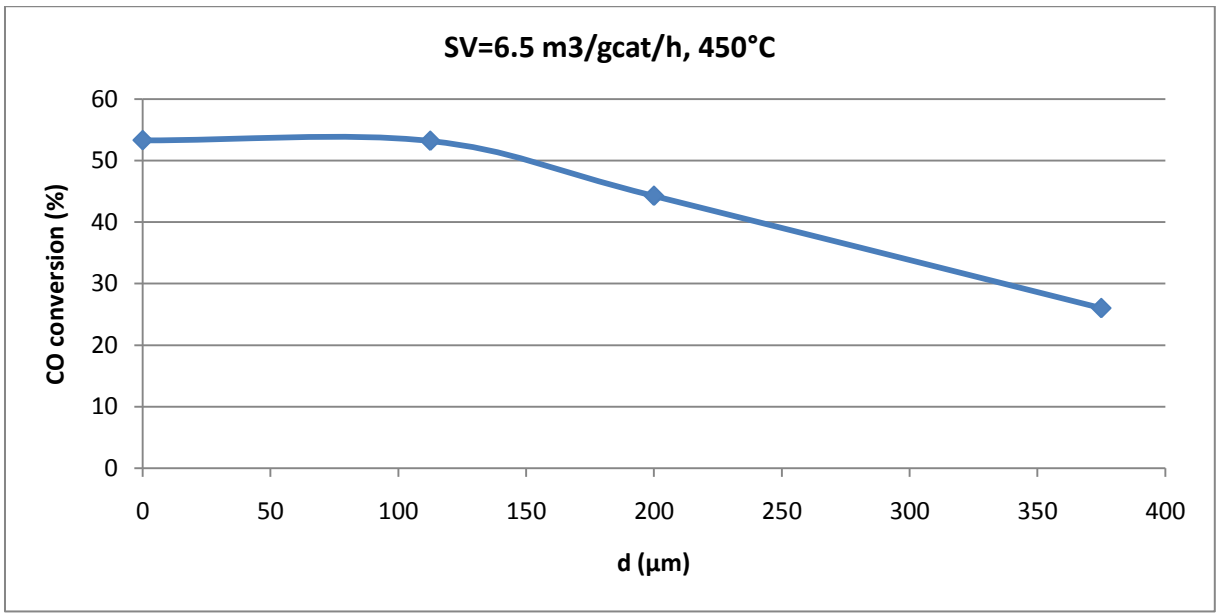

Figure 17: Evolution of the CO conversion with respect to the mean particle size

It means that there are no internal diffusion limitations for particle size under 110µm. The 150µm<d<75µm size distribution was then used, but results with the 500µm<d<250µm are also available.

IV.1.2.External diffusion

The external diffusion has been investigated by working at constant space velocity with three different flowrates and weights with the 150µm<d<75µm.

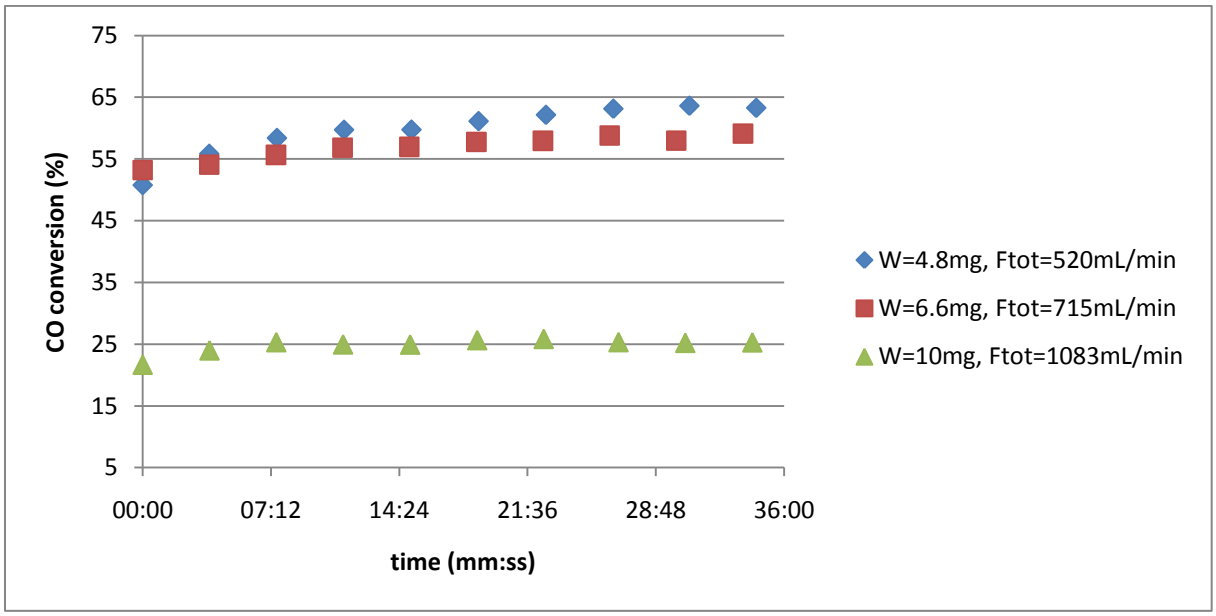

Figure 18: CO conversion with three different loads at constant space velocity (450°C, 0.5bars, SV=6.5$m^3.g^{-1}_{cat}.h^{-1}$, 15.4%CO, 46.2%H_2O, 11.9%H_2, 7%CO_2, 19.6%He)

Figure 18 shows that for low flowrates the external diffusion limitations can be neglected. For high flowrate it appeared that the conversion was much lower. It may indicate that the thermal diffusion into the catalyst is not effective due to the high flowrate of the gases. In that case the catalyst surface is at a lower temperature, leading to a lower conversion.

IV.2.Methanation

Ni is a good catalyst for methanation [36].Therefore a significant fraction of CO and of hydrogen was transformed into methane, decreasing the hydrogen production. The methanation was hardly reduced with the 30%Ni10%Co catalyst, as seen on Figure 19.

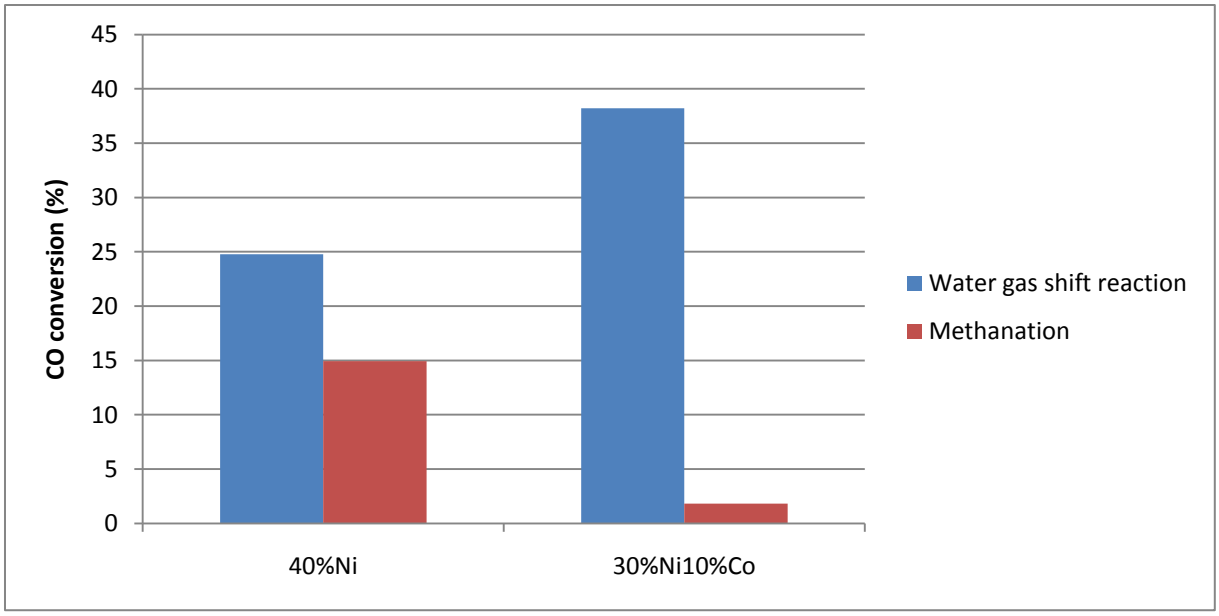

Figure 19: Comparison of two catalysts with regards to methanation (450°C, 0.5bars, SV=6.5$m^3.g^{-1}_{cat}.h^{-1}$, 9.6%CO, 38.5%H_2O, 17.3%H_2, 15.4%CO_2, 19.2%He)

Consequently the hydrogen production is improved with the addition of cobalt in the nickel based catalyst.

IV.3.Kinetics of the WGS

All the experiments for kinetic data have been made at low conversion (<25%) and each point corresponds to several readings after the concentrations were stable. The equilibrium approach β was found at most equal to 0.2, and the reaction rate was corrected by its value.

IV.3.1.Reaction orders

The reaction orders of hydrogen and carbon monoxide were analyzed for one composition of the catalyst, 40% Ni, in order to identify the most probable mechanism for the water gas shift reaction at high temperature.

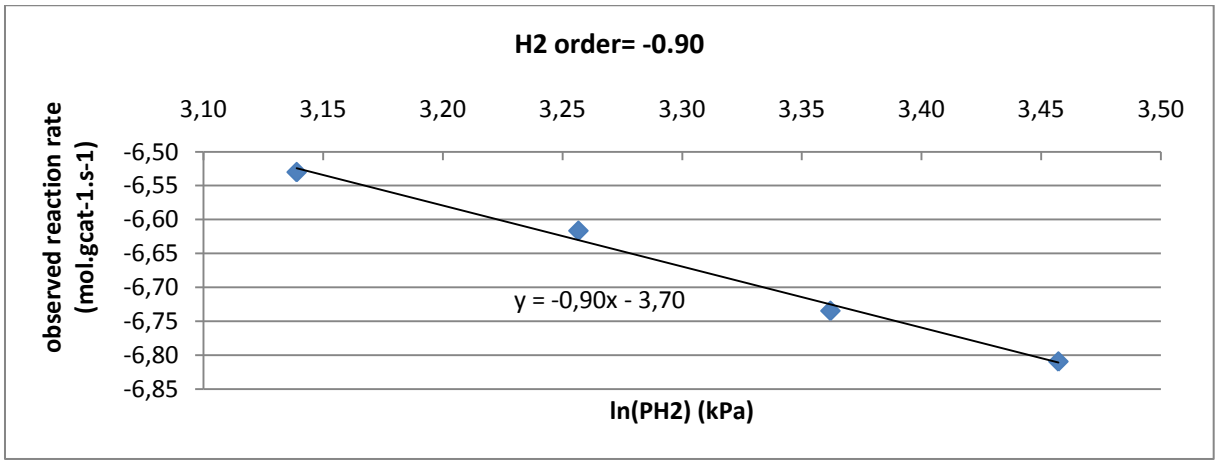

Figure 20: H_2 reaction order (450°C, 0.5bars, SV=6.5$m^3.g^{-1}_{cat}.h^{-1}$, 9.6%CO, 38.5%H_2O, 17.3-21.2%H_2, 15.4%CO_2, 15.4-19.2%He)

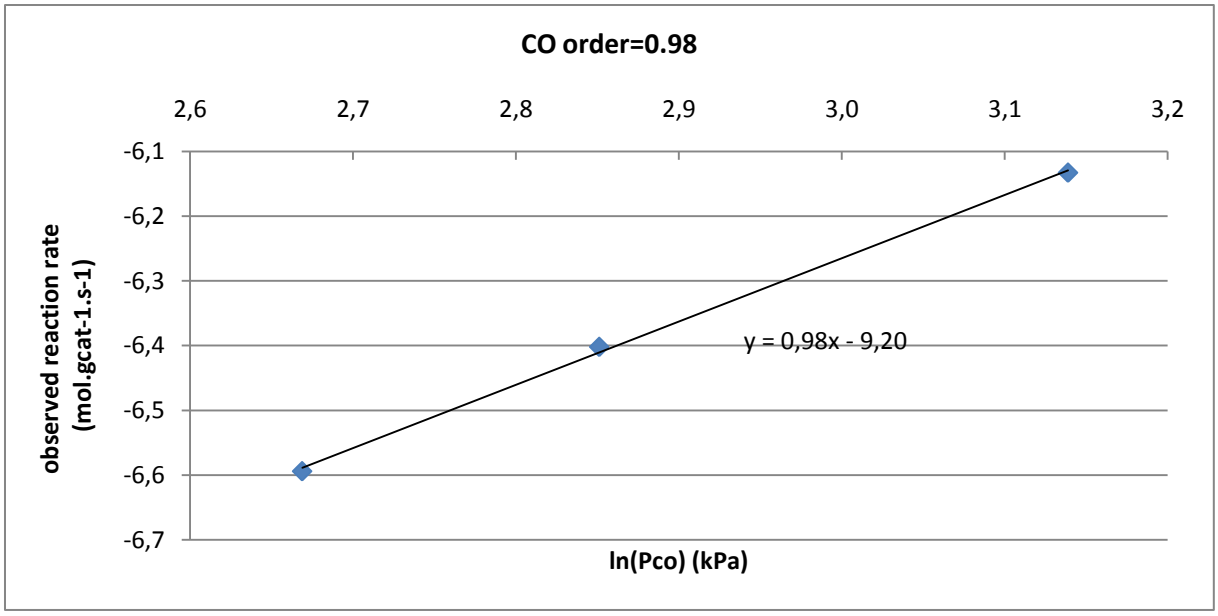

Figure 21: CO reaction order (450°C, 0.5bars, SV=6.5$m^3.g^{-1}_{cat}.h^{-1}$, 9.6-15.4%CO, 38.5%H_2O, 17.3%H_2, 15.4%CO_2, 13.5-19.2%He)

The reaction orders of hydrogen and carbon monoxide match with only one possible reaction rate:

$$r_5 = \frac{\frac{k_5}{K_5 K_6} P_{CO} P_{H_2O} P_{H_2}^{-1} (1-\beta)}{(1 + K_1 P_{CO} + K_2 P_{H_2O} + \frac{P_{CO_2}}{K_6} + \sqrt{\frac{P_{H_2}}{K_7}} + K_2 K_3 K_4 K_7 \frac{P_{H_2O}}{P_{H_2}} + K_2 K_3 \sqrt{K_7} \frac{P_{H_2O}}{\sqrt{P_{H_2}}})^2}$$

It corresponds to the redox mechanism with the CO_2 formation (step 5) as the rate determining step:

(1) CO + * ↔ CO*
(2) H_2O + * ↔ H_2O*
(3) H_2O* + * ↔ OH* + H*
(4) OH* + * ↔ O* + H*
(5) CO* + O* ↔ CO_2* + *
(6) CO_2* ↔ CO_2 + *
(7) 2H* ↔ H_2 + 2*

The expression found by Xu and Froment [38] is similar at low pressure:

$$r = k \frac{P_{CO} P_{H_2O} P_{H_2}^{-1} (1 - \frac{P_{CO_2} P_{H_2}}{K P_{CO} P_{H_2O}})}{(1 + K_{CO} P_{CO} + K_{H_2} P_{H_2} + K_{CH_4} P_{CH_4} + K_{H_2O} \frac{P_{H_2O}}{P_{H_2}})}$$

IV.3.2.Activation energy

In order to have the activation energy, measurements were made at different temperature and ln(rate) was plot with regards to 1/T. The results are shown on Figure 22:

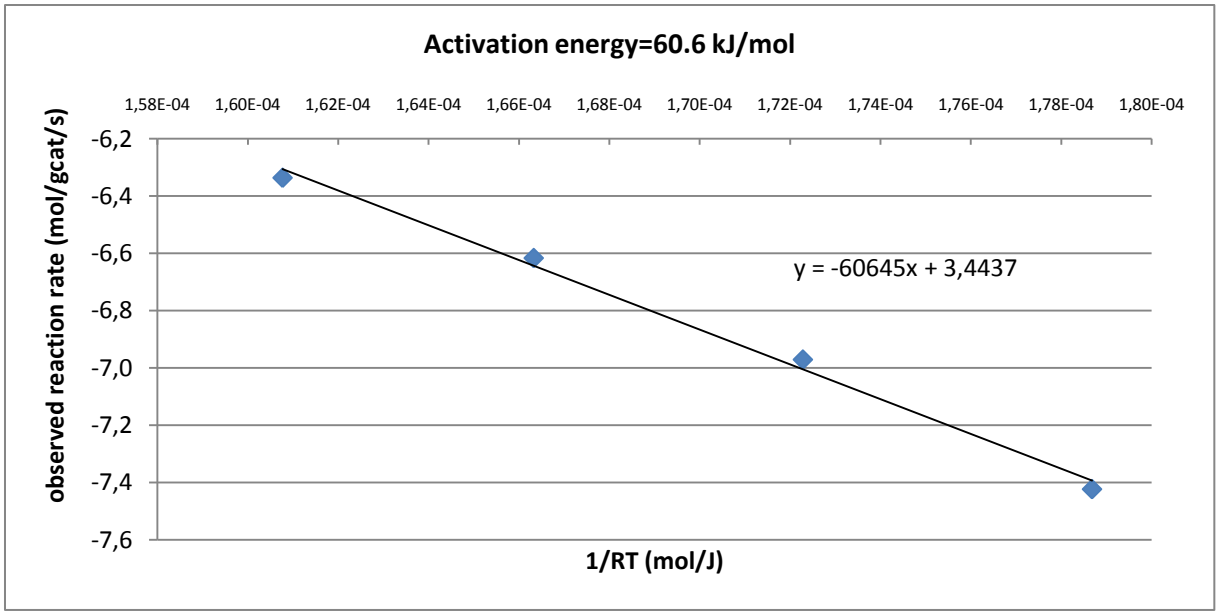

Figure 22: Arrhenius plot (400-475°C, 0.5bars, SV=6.5$m^3.g^{-1}_{cat}.h^{-1}$, 9.6%CO, 38.5%H_2O, 17.3%H_2, 15.4%CO_2, 19.2%He)

This result is similar to the value found by Xu and Froment over nickel [38], 67.13kJ/mol.

IV.3.2.Kinetics under diffusion control

Under diffusion control, the apparent orders and activation energy are different from the actual values under kinetic control. Table 14 summarizes the theoretical effects of internal and external diffusion on these parameters:

Controlling regime	apparent order	apparent activation energy
kinetic	n	E
external diffusion	1	0
internal diffusion	(n+1)/2	E/2

Table 14: Apparent orders and activation energy under diffusion control

The following figure shows data under internal diffusion only, which means with a bigger particle size (500µm<d<250µm).

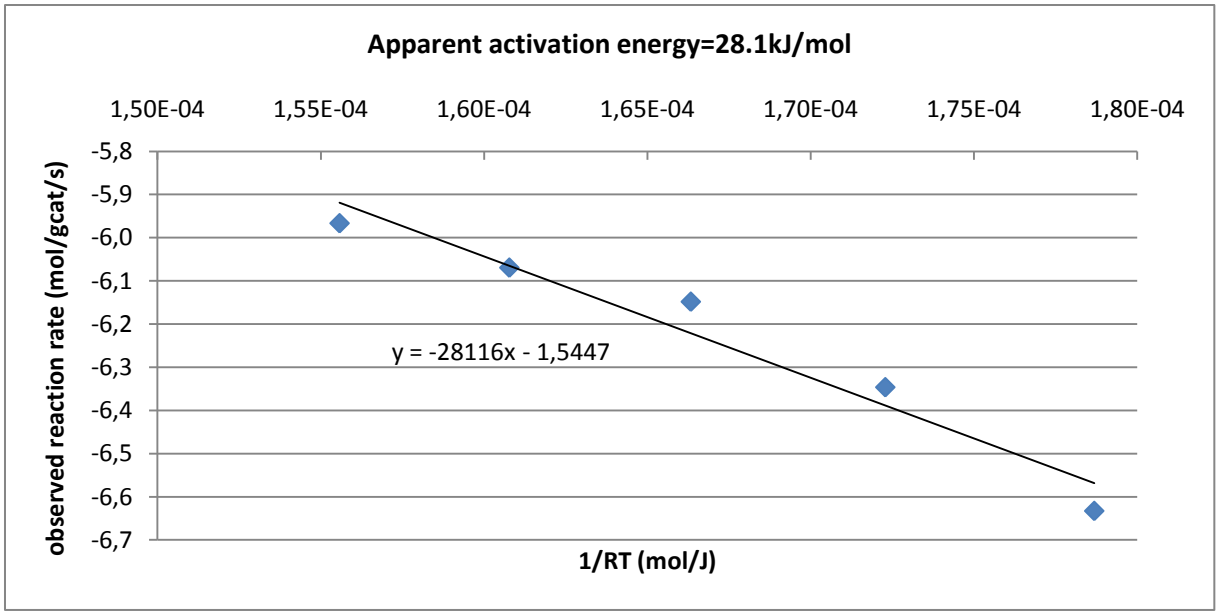

Figure 23: activation energy under internal diffusion control (400-500°C, 0.5bars, SV=6.5$m^3.g^{-1}_{cat}.h^{-1}$, 15.2%CO, 45.5%H_2O, 11.7%H_2, 6.9%CO_2, 20.7%He)

The apparent activation energy found under internal diffusion control is approximately the half of the activation energy found under kinetic control.

Conclusion

The water gas shift reaction has been studied at high temperature over a nickel catalyst in order to determine its kinetic parameters. The activation energy found in this study is in good agreement with previous studies, and the expression of the rate is similar too. The water gas shift reaction is following the redox mechanism at high temperature over nickel. During this study, it appeared that gas phase reaction and diffusion limitations were barriers to a good kinetic study. Furthermore the addition of cobalt in the nickel catalyst showed a better selectivity for the water gas shift reaction compared to the methanation which occurs in a relatively big amount on a nickel catalyst. To complete this work a more comprehensive study of the water gas shift reaction over different nickel-cobalt catalysts could be done.

Nomenclature

ΔH : enthalpy (J/mol)

K: equilibrium constant of the water gas shift reaction

T: temperature (K)

Ea: activation energy (J/mol)

P_i: partial pressure of component i

R: perfect gas constant

k_i: rate constant of step i

K_i: equilibrium constant of step i

r_i: rate of reaction i (mol/kg/s)

X_{wgs}: conversion of CO into CO_2

X_{meth}: conversion of CO into CH_4

F: molar flow (mol/s)

W: weight of the catalyst (kg)

References

[1] Podolski, W. F., & Kim, Y. G. (1974). Modeling the water-gas shift reaction. *Industrial and Engineering Chemistry: Process Design and Development, 13*(4), 415-421

[2] Newsome, D. S. (1980). WATER-GAS SHIFT REACTION. *Catalysis Reviews Softcover Ed., 21*(2), 275-281, *Boreskov, G.K. (1966) Forms of oxygen bonds on the surface of oxidation catalysts, Disc. Faraday Soc., 1966, 41, 263–276*

[3] *Boreskov, G.K.; Yureva, T.M., Morozov, N.M., Sergeeva A.S., Kinet. Katal, 11, 1476 (1970), Temkin, M. I. (1979). The kinetics of some industrial heterogeneous catalytic reactions, Advances in Catalysis 28 (C), pp. 173-291*

[4] *Bohlbro, H. (1964). The kinetics of the water-gas conversion IV. influence of alkali on the rate equation. Journal of Catalysis, 3(3), 207-215*

[5] *Chinchen, G. C., Logan, R. H., & Spencer, M. S. (1984). Water-gas shift reaction over an iron oxide/chromium oxide catalyst. I: Mass transport effects. Applied Catalysis, 12(1), 69-88*

[6] *Chinchen, G. C., Logan, R. H., & Spencer, M. S. (1984). Water-gas shift reaction over an iron oxide/chromium oxide catalyst. II: Stability of activity. Applied Catalysis, 12(1), 89-96*

[7] *Chinchen, G. C., Logan, R. H., & Spencer, M. S. (1984). Water-gas shift reaction over an iron oxide/chromium oxide catalyst. III: Kinetics of reaction. Applied Catalysis, 12(1), 97-103*

[8] Koryabkina, N. A., Phatak, A. A., Ruettinger, W. F., Farrauto, R. J., & Ribeiro, F. H.(2003). Determination of kinetic parameters for the water-gas shift reaction on copper catalysts under realistic conditions for fuel cell applications. *Journal of Catalysis, 217*(1), 233-239

[9] Stevens, RW; Shamsi, A; Carpenter, S; Siriwardane, R. 2010. Sorption-enhanced water gas shift reaction by sodium-promoted calcium oxides. *Fuel* 89 (6):1280-1286

[10] Barelli, L; Bidini, G; Gallorini, F; Servili, S. 2008. Hydrogen production through sorption-enhanced steam methane reforming and membrane technology: A review. *Energy* 33 (4):554-570

[11] Mendes, D; Mendes, A; Madeira, LM; Iulianelli, A; Sousa, JM; Basile, A. 2010. The water-gas shift reaction: from conventional catalytic systems to Pd-based membrane reactors - a review. *Asia-Pacific Journal Of Chemical Engineering* 5 (1):111-137

[12] A. Criscuoli, A. Basile, E. Drioli. 2000. An analysis of the performance of membrane reactors for the water-gas shift reaction using gas feed mixtures, *Catalysis Today* 56 (1-3): 53-64

[13] Voecks G, DOE consultant and coordinator of the contamination group. The development of hydrogen fuel quality specification, Canada-USA PEM network research workshop, in Vancouver, BC, Canada; Feb. 16-17, 2009

[14] Divisek, J; Oetjen, HF; Peinecke, V; Schmidt, VM; Stimming, U. 1998. Components for PEM fuel cell systems using hydrogen and CO containing fuels. *Electrochimica Acta* 43 (24):3811-3815

[15] Zamel, N; Li, XG. 2011. Effect of contaminants on polymer electrolyte membrane fuel cells. *Progress In Energy And Combustion Science* 37 (3):292-329

[16] Garcia AC, Paganin VA, Ticianelli EA. CO tolerance of PdPt/C and PdPtRu /C anodes for PEMFC. *Electrochimica Acta* 2008;53:4309-15

[17] Papageorgopoulos DC, Keijzer M, Veldhuis JBJ, de Bruijn FA. CO tolerance of Pd-rich platinum palladium carbon-supported electrocatalysts. *Journal of Electrochemical Society* 2002;149:A1400-4

[18]Callaghan, C., Fishtik, I., Datta, R., Carpenter, M., Chmielewski, M., & Lugo, A. (2003). An improved microkinetic model for the water gas shift reaction on copper. *Surface Science, 541*(1-3), 21-30

[19]Nakamura, J., Campbell, J. M., & Campbell, C. T. (1990). Kinetics and mechanism of the water-gas shift reaction catalysed by the clean and cs-promoted cu(110) surface: A comparison with cu(111). *Journal of the Chemical Society, Faraday Transactions, 86*(15), 2725-2734

[20]Ernst, K. , Campbell, C. T., & Moretti, G. (1992). Kinetics of the reverse water-gas shift reaction over cu(110). *Journal of Catalysis, 134*(1), 66-74

[21]Thinon, O., Rachedi, K., Diehl, F., Avenier, P., & Schuurman, Y. (2009). Kinetics and mechanism of the water-gas shift reaction over platinum supported catalysts. *Topics in Catalysis, 52*(13-20), 1940-1945

[22]Hla, S. S., Park, D., Duffy, G. J., Edwards, J. H., Roberts, D. G., Ilyushechkin, A., et al. (2009). Kinetics of high-temperature water-gas shift reaction over two iron-based commercial catalysts using simulated coal-derived syngases. *Chemical Engineering Journal, 146*(1), 148-154

[23]Phatak, AA; Koryabkina, N; Rai, S; Ratts, JL; Ruettinger, W; Farrauto, RJ; Blau, GE; Delgass, WN; Ribeiro, FH. 2007. Kinetics of the water-gas shift reaction on Pt catalysts supported on alumina and ceria. *Catalysis Today* 123 (1-4):224-234

[24]Leppelt, R; Schumacher, B; Plzak, V; Kinne, M; Behm, RJ. 2006. Kinetics and mechanism of the low-temperature water-gas shift reaction on Au/CeO2 catalysts in an idealized reaction atmosphere. *Journal Of Catalysis* 244 (2):137-152

[25]Gokhale, A.A., Dumesic, J. A., Mavrikakis, M.M. (2008) On the mechanism of low temperature water gas shift reaction on copper. *J. Amer. Chem. Soc*., 130, 1402–1414

[26]Liu, P; Rodriguez, JA. 2007. Water-gas-shift reaction on metal nanoparticles and surfaces. *Journal Of Chemical Physics* 126 (16)].

[27]Shi, XR; Wang, SG; Hu, J; Wang, H; Chen, YY; Qin, ZF; Wang, JG. 2009. Density functional theory study on water-gas-shift reaction over molybdenum disulfide. *Applied Catalysis A-General* 365 (1):62-70

[28]Chen, Y. -., Dong, M., Wang, J., & Jiao, H. (2010). On the role of a cobalt promoter in a water-gas-shift reaction on co-MoS2. *Journal of Physical Chemistry C, 114*(39), 16669-16676

[29]Rhodes, C., Hutchings, G. J., & Ward, A. M. (1995). Water-gas shift reaction: Finding the mechanistic boundary. *Catalysis Today, 23*(1), 43-58

[30]Boon, J., Van Dijk, E., Pirgon-Galin, Ö, Haije, W., & Van Den Brink, R. (2009). Water-gas shift kinetics over fecr-based catalyst: Effect of hydrogen sulphide. *Catalysis Letters, 131*(3-4), 406-412

[31]Rhodes, C; Williams, BP; King, F; Hutchings, GJ. 2002. Promotion of Fe3O4/Cr2O3 high temperature water gas shift catalyst. *Catalysis Communications* 3 (8):381-384

[32]Coleman, J. S., Zhang, M., VanNatter, R. M., & Lund, C. R. F. 2010. Copper promotion of high temperature shift. *Catalysis Today*

[33] Reddy, GK; Gunasekera, K; Boolchand, P; Dong, JH; Smirniotis, PG. 2011. High Temperature Water Gas Shift Reaction over Nanocrystalline Copper Codoped-Modified Ferrites. *Journal Of Physical Chemistry C* 115 (15):7586-7595

[34]Natesakhawat, S; Wang, XQ; Zhang, LZ; Ozkan, US. 2006. Development of chromium-free iron-based catalysts for high-temperature water-gas shift reaction. *Journal Of Molecular Catalysis A-Chemical* 260 (1-2):82-94

[35]Lee, JY; Lee, DW; Lee, KY; Wang, Y. 2009. Cr-free Fe-based metal oxide catalysts for high temperature water gas shift reaction of fuel processor using LPG. *Catalysis Today* 146 (1-2):260-264

[36]Sung Ho Kim, Suk-Woo Nam, Tae-Hoon Lim, Ho-In Lee (2008), Effect of pretreatment on the activity of Ni catalyst for CO removal reaction by water-gas shift and methanation*, Applied Catalysis B: Environmental, 81(1-2),* 97-104

[37]Hwang, K., Lee, C. & Park, J. (2011). Advanced nickel metal catalyst for water-gas shift reaction. *Journal of Power Sources, 196*(3), 1349-1352

[38]Xu, Jg; Froment, Gf. 1989. Methane Steam Reforming, Methanation And Water-Gas Shift .1. Intrinsic Kinetics. *Aiche Journal* 35 (1):88-96

[39]Twigg, MV; Spencer, MS. 2001. Deactivation of supported copper metal catalysts for hydrogenation reactions. *Applied Catalysis A-General* 212 (1-2):161-174

[40]Hilaire, S; Wang, X; Luo, T; Gorte, RJ; Wagner, J. 2001. A comparative study of water-gas-shift reaction over ceria supported metallic catalysts. *APPLIED CATALYSIS A-GENERAL* 215 (1-2):271-278

[41]Li, Y., Fu, Q., & Flytzani-Stephanopoulos, M. (2000). Low-temperature water-gas shift reaction over cu- and ni-loaded cerium oxide catalysts. *Applied Catalysis B: Environmental, 27*(3), 179-191

[42]Grenoble, D. C., Estadt, M. M., & Ollis, D. F. (1981). The chemistry and catalysis of the water gas shift reaction. 1. the kinetics over supported metal catalysts. *Journal of Catalysis, 67*(1), 90-102

[43]Kalamaras, CM; Americanou, S; Efstathiou, AM. 2011. "Redox" vs "associative formate with -OH group regeneration" WGS reaction mechanism on Pt/CeO2: Effect of platinum particle size. *Journal Of Catalysis* 279 (2):287-300

[44]Ricote, S; Jacobs, G; Milling, M; Ji, YY; Patterson, PM; Davis, BH. 2006. Low temperature water-gas shift: Characterization and testing of binary mixed oxides of ceria and zirconia promoted with Pt. *Applied Catalysis A-General* 303 (1):35-47

[45]Gonzalez, ID; Navarro, RM; Wen, W; Marinkovic, N; Rodriguez, JA; Rosa, F; Fierro, JLG. 2010. A comparative study of the water gas shift reaction over platinum catalysts supported on CeO2, TiO2 and Ce-modified TiO2. *Catalysis Today* 149 (3-4):372-379

[46]Rodriguez, J. A., Liu, P., Hrbek, J., Evans, J., & Pérez, M. (2007). Water gas shift reaction on cu and au nanoparticles supported on CeO 2(111) and ZnO(0001): Intrinsic activity and importance of support interactions. *Angewandte Chemie - International Edition, 46*(8), 1329-1332

[47]Rodríguez, J. A., Evans, J., Graciani, J., Park, J. -., Liu, P., Hrbek, J., et al. (2009). High water-gas shift activity in TiO2(110) supported cu and au nanoparticles: Role of the oxide and metal particle size. *Journal of Physical Chemistry C, 113*(17), 7364-7370

[48]Rodríguez, J. A., Liu, P., Hrbek, J., Pérez, M., & Evans, J. (2008). Water-gas shift activity of au and cu nanoparticles supported on molybdenum oxides. *Journal of Molecular Catalysis A: Chemical, 281*(1-2), 59-65

[49]Park, J. B., Graciani, J., Evans, J., Stacchiola, D., Ma, S., Liu, P., et al. (2009). High catalytic activity of Au/CeOx/TiO2(110) controlled by the nature of the mixed-metal oxide at the

nanometer level. *Proceedings of the National Academy of Sciences of the United States of America, 106*(13), 4975-4980

[50]Alstrup, I. (1995). On the kinetics of co methanation on nickel surfaces. *Journal of Catalysis, 151*(1), 216-225

[51]Ojeda, M., Nabar, R., Nilekar, A. U., Ishikawa, A., Mavrikakis, M., & Iglesia, E. (2010). CO activation pathways and the mechanism of fischer-tropsch synthesis. *Journal of Catalysis, 272*(2), 287-297

Appendix 1: Risk assessment

NTNU	Risk assessment	Prepared by	Number	Date
HSE/KS		HSE section	HMSRV-26/03	01.12.2006
		Approved by	Page	Replaces
		The Rector	1 out of 1	15.12.2003

Unit: **Date:**

Line manager:

Participants in the risk assessment (including their function):

Activity from the identification process form	Potential undesirable incident/strain	Likelihood:	Consequence:			Risk value	Comments/status Suggested measures
		Likelihood (1-4)	Human (1-4)	Environment (1-4)	Economy/ materiel (1-4)		
Move activity twin plant start up	problem with temperature control	2	1	1	2	2/2/4	- alarm if T > 800°C
	problem with pressure control P sensor	2	1	1	2	2/2/4	- alarm - inlet close if P is high
	gas leaking	3	1	1	1	3	- gas detectors in the lab
	problem with water level control	1	1	1	1	1	- alarm

Likelihood, e.g.:
1. *Minimal*
2. *Low*
3. *High*
4. *Very high*

Consequence, e.g.:
1. *Relatively safe*
2. *Dangerous*
3. *Critical*
4. *Very critical*

Risk value (each one to be estimated separately):
Human = Likelihood x Human Consequence
Environmental = Likelihood x Environmental consequence
Financial/material = Likelihood x Consequence for Economy/materiel

Appendix 3: Health, safety and environment

Some gases used in this set-up have to be manipulated with precaution:

- Carbon monoxide is highly toxic for humans, is colorless and odorless. A CO detector is in the room close to the set-up, and portable devices are available to detect any leakage of carbon monoxide.
- Hydrogen is highly explosive in air. Its presence can be detected by the portable devices to avoid any leakage.
- Carbon dioxide is toxic too.

To avoid releasing the gases in the room, the outlet of the reactor and the gas chromatography are connected to the ventilation.